SEDIMENTOLOGY the journal of the International Association of Sedimentologists

Sedimentology (2021) **68**, 1674–1697 doi: 10.1111/sed.12735

Reconstruction of bedform dynamics controlled by supercritical flow in the channel–lobe transition zone of a deep-water delta (Sant Llorenç del Munt, north-east Spain, Eocene)

GEORGE POSTMA*, JÖRG LANG†, DAVID C. HOYAL‡, JUAN J. FEDELE‡, TIMOTHY DEMKO‡, VITOR ABREU§ and KERIANN H. PEDERSON‡

**Faculty of Geosciences, Utrecht University, PO Box 80.021, 3508TA, Utrecht, the Netherlands (E-mail: g.postma@uu.nl)*

†Institut für Geologie, Leibniz Universität Hannover, Callinstraße 30, 30167 Hannover, Germany

‡ExxonMobil Upstream Research Company, 22777 Springwoods Village Parkway Spring, Houston, TX 77389, USA

§Act-Geosciences, 344 W 22nd St. Houston, TX 77008, USA

Associate Editor – Arnoud Slootman

ABSTRACT

Stable supercritical-flow bedform phases under two-dimensional steady flow are geometrically simple and include long-wavelength cyclic steps at high Froude numbers and antidunes characterized by in-phase flow that is near critical. Less well understood are the transitional bedform phases at the boundaries of the stable bedform fields and bedforms developing in complex flow geometries like the channel–lobe transition zone. This complexity is exacerbated by the fact that natural flows are never steady. Stable antidune bedforms may be reworked by temporally increasing discharge into chute and pool, and cyclic step and chute and pool fields will be reworked into antidunes if discharge is sufficiently decreasing. In addition, the channel–lobe transition zone is continuously evolving in space and time due to the influence of solitary hydraulic jumps at the channel mouth on channel extension and back stepping. This detailed outcrop study of a deep-water delta slope belonging to the Eocene Sant Llorenç del Munt clastic wedge exposed near El Pont de Vilomara (north-east Spain), tackles the complex bedform architecture problems by applying a method previously developed for fluvial deposits. Analysis of surfaces traced on high-definition, drone-derived in-strike images combines architectural studies with facies analysis. Set boundaries of the bedforms were thus established, revealing the upslope migration of hydraulic jump zones and the intricate stacking of antidunes and solitary, mouthbar related chute and pool like structures. Further analysis of the stacking of bedforms and bounding surfaces provide evidence that deposition occurred in a relatively short (few hundreds of metres) channel–lobe transition zone at the base of the delta slope. The usefulness of the bounding surface hierarchy approach for turbidite deposits lies in the careful evaluation of the spatial extent of bounding surfaces, which are easily overlooked in complex architectures such as those created in the channel–lobe transition zone.

Keywords Bedform preservation, bedforms, bounding surface hierarchy, channel–lobe transition zone, deepwater delta, supercritical flow, turbidity currents.

INTRODUCTION

In contrast to supercritical-flow bedforms created by rivers, those originating from density underflows have not received parallel attention, in part because these flows are difficult to study from a sedimentological perspective in the modern environment (Fedele *et al.*, 2016). Recent outcrop studies, new high-resolution sea floor bathymetric and seismic data and recent laboratory experimental work suggest not only a wide variety of sediment-gravity flow related bedforms in size and in shape (Hand, 1974; Spinewine *et al.*, 2009; Hughes Clarke *et al.*, 2012; Cartigny *et al.*, 2014; Covault *et al.*, 2014; Postma *et al.*, 2014; Cartigny & Postma, 2016; Fedele *et al.*, 2016; Hughes Clarke, 2016; Massari, 2017; Hage *et al.*, 2018; Cornard & Pickering, 2019), but also that few studies exist that deal with the preservation of these bedforms (Slootman & Cartigny, 2020; Vendettuoli *et al.*, 2019).

While work on deep-water supercritical-flow bedforms in modern environments is increasing and images of bedform morphology on deep-water delta slopes (Hughes Clarke *et al.*, 2012; Hughes Clarke, 2016), in canyons (Paull *et al.*, 2011, 2018) and in the channel-lobe-transition-zone (CLTZ; Gervais *et al.*, 2004; Deptuck *et al.*, 2008) started to more clearly emerge in the last decade, few of these studies have linked sea floor observations to sedimentary facies and architecture (Hage *et al.*, 2018; Vendettuoli *et al.*, 2019). However, these studies do provide valuable well-supported bedform diagnostic recognition criteria for sedimentologists to use at the outcrop scale. Deep-water supercritical-flow bedform recognition in outcrop is complicated not only because of their size (wavelengths typically in the order of tens of metres up to kilometres, see Cartigny & Postma, 2016) but also because of their three-dimensional structure and upslope migration pattern, with many truncation surfaces producing structures with variable preservation potential, as inferred mostly from experimental work (Alexander *et al.*, 2001; Cartigny *et al.*, 2014; Fedele *et al.*, 2016; Pohl, 2019). As pointed out by recent studies, large supercritical-flow bedform geometries in outcrop might have been misinterpreted by being attributed to small channels (Lang *et al.*, 2017; Ono & Plink-Björklund, 2018; Slootman *et al.*, 2019b).

Hence, there is still much to learn about the architecture and facies of supercritical-flow bedforms from outcrop studies in almost all kinds of palaeoenvironments, such as outwash plains, narrow seaways (straits), deltas, submarine canyons, volcanic and glaciolacustrine settings (e.g. Ponce & Carmona, 2011; Lang & Winsemann, 2013; Postma *et al.*, 2014, 2016; Postma & Kleverlaan, 2018; Ventra *et al.*, 2015; Bain & Hubbard, 2016; Dietrich *et al.*, 2016; Lang *et al.*, 2017; Ono & Plink-Björklund, 2018; Slootman & Cartigny, 2020; Slootman *et al.*, 2019a,b, this volume) as important modifications of idealized bedform morphologies exist due to variable discharge, net aggradation rates and the translation of the depo-centre, which all result in different preservation styles (Lang *et al.*, 2017). Therefore, establishing diagnostic criteria for supercritical-flow bedforms such as, for example, backset bedding is paramount.

This paper presents a detailed outcrop study of supercritical-flow bedforms in a CLTZ of a deep-water delta slope of the Eocene Sant Llorenç del Munt near Montserrat (north-east Spain, e.g. Marzo & Anadón, 1988). To do justice to the complex structure of amalgamated supercritical-flow bedforms, their bounding surface (BS) hierarchy was studied following a methodology analogous to that developed by Miall (1985) for fluvial deposits. Objectives of this study are to evaluate the morphodynamics and resultant style of preservation in the CLTZ. With this study, the usefulness of the BS hierarchy approach for unravelling the various types of supercritical-flow bedforms is demonstrated.

GEOLOGICAL SETTING

The Montserrat and Sant Llorenç del Munt clastic wedges are located along the south-eastern margin of the Ebro foreland basin adjacent to the Catalan Coastal Ranges, an Alpine structural unit running parallel to the Mediterranean coast in the north-eastern part of the Iberian Peninsula (Fig. 1A).

The formation and evolution of the Montserrat and Sant Llorenç clastic wedges are closely related to the tectonic evolution of the adjoining Palaeogene Catalan Coastal Range, which comprises a transpressive chain characterized by a frontal thrust formed from the propagation of a large, out of sequence thrust through the forelimb of a syncline–anticline pair. During the Lutetian, tectonic activity led to the development of coalescing alluvial-fan systems along the Ebro foreland margin. After a regionally

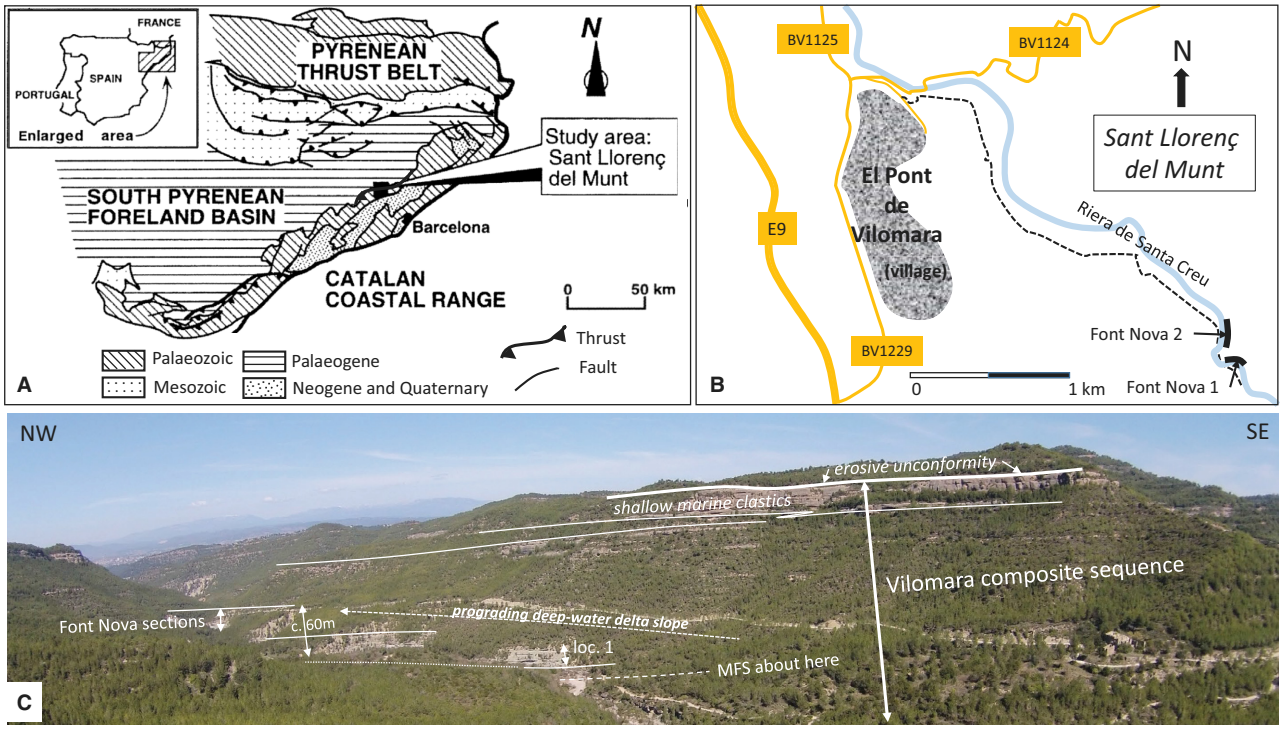

Fig. 1. (A) Geological and locality map of the Eocene clastic alluvial fan and fan-delta wedges of the Sant Llorenç del Munt modified from Steel *et al.*, 2000 and López-Blanco *et al.*, 2000b. (B) Road map to the study localities Font Nova 1 and 2 in the river valley of Riera de Santa Creu near El Pont de Vilomara. (C) The Vilomara composite sequence illustrating continental to marine transitions and deep-water delta clinoforms developing above the maximum flooding surface (MFS; López-Blanco *et al.*, 2000b; Steel *et al.*, 2000). From about Locality 1 (described in Postma *et al.*, 2016) clinoforms can be seen prograding northward. The measured stratigraphic thickness from the base of Locality 1 to the top of Font Nova 2 section is about 60 m.

widespread Bartonian relative sea-level rise, these alluvial-fan systems evolved to fan deltas prograding in a north-west to north-east direction (Marzo & Anadón, 1988, and references therein).

Combined biostratigraphic and palaeomagnetic studies (summarized in López-Blanco *et al.*, 2000c) suggest that the alluvial-fan (uppermost Lutetian) and the fan-delta (Bartonian) deposits forming the Montserrat Conglomerate span as much as 4.4 Myr, from 41.6 to 37.2 Ma. During that time span, the sedimentation and total subsidence rates increased through time, reflected by rapid growth of the topographic relief in response to modest shortening and considerable vertical bedrock uplift. The prevailing warm and humid climate during that period resulted in increased denudation rates and sediment supply to the shoreline resulting in the formation of clastic alluvial fan and fan-delta sediment wedges.

The here studied sections belong to the Vilomara composite sequence of the Sant Llorenç del Munt fan-delta complex, which are nicely exposed in the Font Nova outcrops in the Riera de Santa Creu river valley (Fig. 1B) near the village El Pont de Vilomara. The Vilomara sequence is 133 m thick and comprises at its base a transgressive sequence tract deposited on top of a carbonate platform and a regressive sequence tract, which is shown in Fig. 1C. Age of the Vilomara composite sequence is approximately 38 Ma (López-Blanco *et al.*, 2000b; Steel *et al.*, 2000; Cabello *et al.*, 2010). The entire transgressive–regressive cycle spans about 90 kyr of time based on magnetostratigraphy and biostratigraphy studies on the marine and terrestrial strata of the Monserrat (López-Blanco *et al.*, 2000b), and based on physical correlation with the Llorenç del Munt sections (López-Blanco *et al.*, 2000a).

The estimated thickness of the regressive part is more than 60 m in the Casa Nova section (López-Blanco *et al.*, 2000a), and the authors estimate that this is more than 80 m near the more northerly situated Font Nova locality (see

Fig. 1C), which would mean a water depth of at least 80 m if no allowance is made for compaction. Thus the delta can be classified as a prograding deep-water delta (Postma, 1990), inferred to be fed by an alluvial fan or braided-river system.

The subaqueous part of the delta consists predominantly of grey mudstone alternating with sandstone units deposited on the slope and at the base of slope (Fig. 2; e.g. Steel *et al.*, 2000). The sandstone units truncate and onlap the subaqueous delta slope on various scales in channel forms from tens of metres up to a few hundred of metres wide. The detailed internal architecture of the sandy turbidite units in the Vilomara unit is complex and has only been described briefly in Postma *et al.* (2016).

METHODOLOGY

The studied sedimentary units were photographed with a hand-held camera and with a Phantom 4 DJI drone (DJI, Shenzhen, China). The drone was used for in-strike images, herewith reducing the apparent dip problem. The units were logged in detail and grain-size trends were established. Facies descriptions follow the detailed facies schemes of Talling *et al.* (2012) and Postma & Cartigny (2014) and are summarized in the caption of Fig. 3.

For architectural reconstructions of complex sedimentary units, the authors believe it is critical to follow a methodology that honours the hierarchy of truncation (bounding) surfaces. Miall (1985) used the hierarchy of bounding

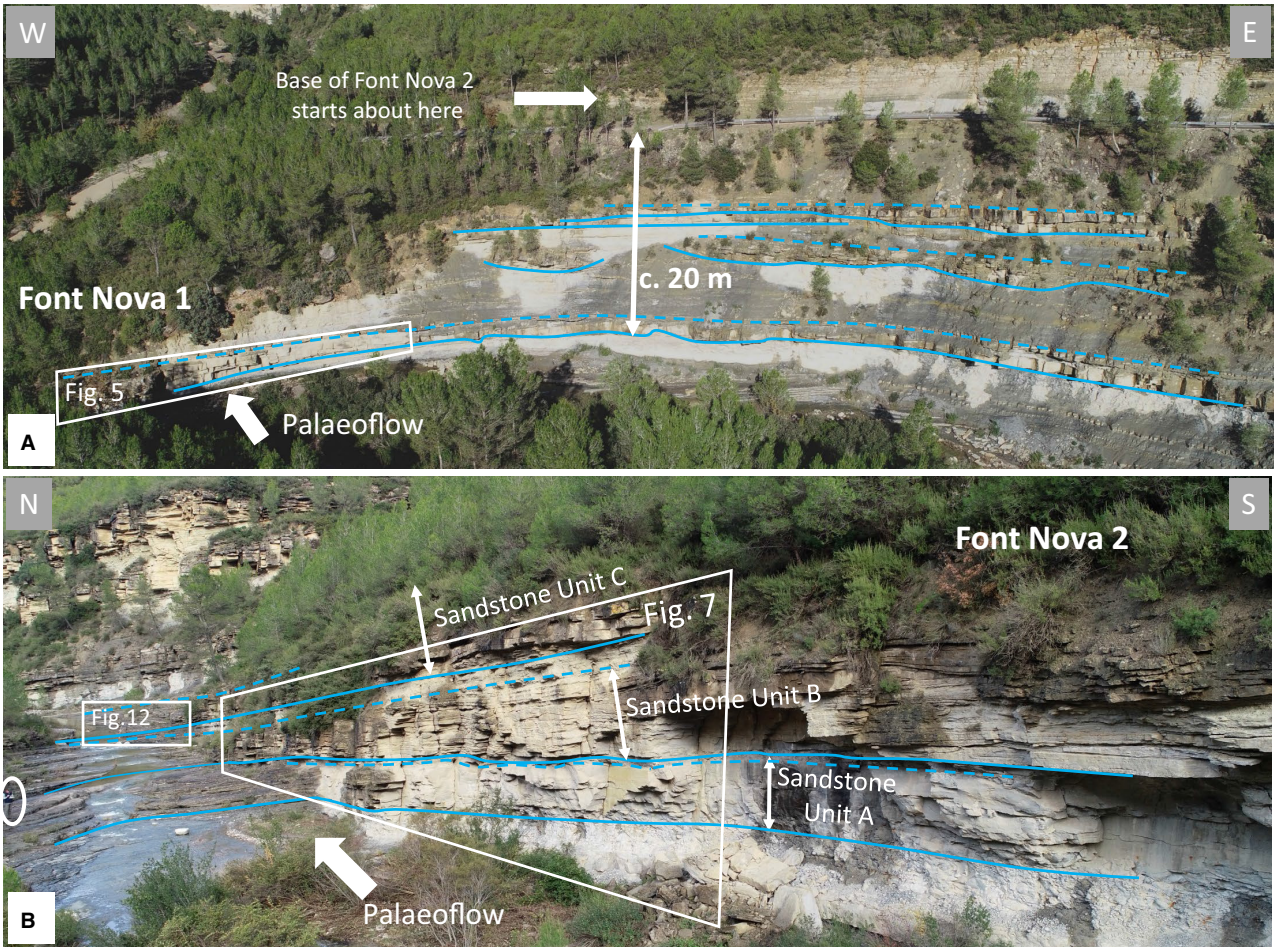

Fig. 2. (A) The Font Nova 1 outcrop showing sandstone bodies incising in blue grey slope mudstone. The section bends from almost perpendicular to longitudinal relative to the palaeoflow at the right hand side of the picture. (B) View towards the north at Font Nova 2 section, which is about in the direction of the general palaeoflow direction (NNE). The Sandstone Units A to C are aligned by solid lines at their sharp, erosive base and dashed blue lines at their top. Sandstone Unit B corresponds to the incising sandstones at the top of Font Nova 1 section approximately at the level indicated by arrow in 2A. Note encircled person for scale (*ca* 1.9 m tall) at the left margin of the image.

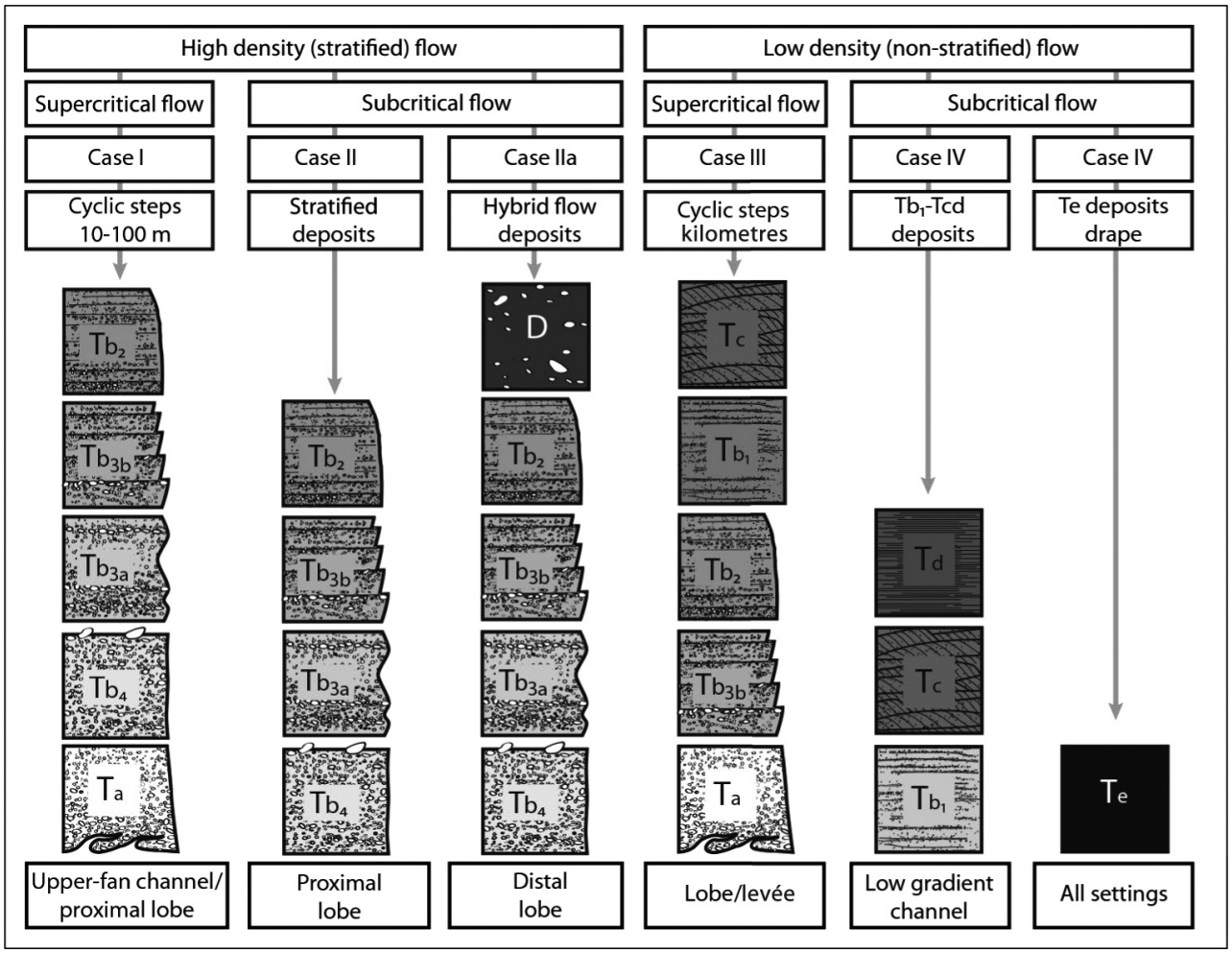

Fig. 3. Summary of flow dynamics and facies for high (cases I and II) and low (cases III and IV) density supercritical and subcritical turbidity currents (from Postma & Cartigny, 2014). Structureless, coarse-tail normally graded Ta unit figures as the most proximal deposit, then the planar laminated unit Tb, the rippled Tc unit and the planar bedded Td units being the most distal with unit Te representing the hemipelagic interval, the final suspension rain that covers the entire turbidite deposit (Bouma, 1962). In this diagram the Tb facies has been expanded for high-density, stratified flows to include the various types of traction carpet facies related to sediment fall out rate and increase of flow speed: massive (structureless) beds (Tb4) with outsized clasts at their top, crude (Tb3a) and spaced stratification (Tb3b), and planar laminations with spacing smaller than 0.5 cm (Tb2). Tb1 refers to plane bed millimetre-laminations characteristic for deposition from low-concentration flows in the upper flow regime. Look for further details and references in Talling *et al.* (2012) and Postma & Cartigny (2014).

surfaces (BS) to determine a relative time and spatial scale for fluvial sedimentary deposits. The Miall (1985) scheme clarified that first-order and second-order surfaces delineate ripple sets and co-sets, respectively, third-order surfaces denote minor bar or bedform sequences, fourth-order sequences point to macroforms like those formed by lateral accretion (point bar) and the fifth-order BS would represent the channel in which the macroform resides.

Miall's (1985) methodology is here adapted for turbidite systems. Since the bed sets that the present work wishes to describe in detail are formed by turbidity currents, and thus represent separate events, the first-order BS delineates primary depositional structures within the turbidite beds, i.e. set boundaries of ripples and truncation surfaces of laminations and traction carpets. Also syn-depositional soft-sediment deformation is regarded here as being of first-order. Second-order BS are the turbidite bed boundaries and represent individual turbidite events. These surfaces show the pinching and thickening of beds, the latter being regarded here as the laminae of

the bedform (cf. Postma *et al.*, 2014). The third-order BS truncates second-order and first-order BS and marks set boundaries, similar to the set boundaries of fluvial dunes and ripples. They are formed by erosion in the trough of a migrating bedform. The fourth-order BS truncate third-order. They delineate storeys in the channel fill and may reflect minor migration of the depocentre (Miall's minor bar migration), but may also reflect exceptional mass transport events (Pickering & Cantalejo, 2015), or a vertical sequence of evolving bedforms related to flow changes (for example, antidunes followed by transitional antidunes changing into cyclic steps). For a schematic presentation of second to fifth-order BS the reader may consult Fig. 5, which is described below. Third-order BS (yellow) envelop bed sets, and fourth-order BS (red) mark stages (storeys) in channel infill. The fifth-order BS (blue) marks the channel boundary. Here, the descriptive terminology developed by Sprague *et al.* (2005) is favoured. For full discussion on terminology for submarine fan channel and lobe sequences the reader is referred to a recent review by Cullis *et al.* (2018).

As described above, the hierarchy thus provides relative temporal and spatial scale to the deposits under investigation. Hence, it is recognized that erosional bounding surfaces always become a conformable bounding surface farther down in the basin, so that eventually all bounding surfaces become conformities in the lobe fringe. At the point where erosion surfaces become conformities the hierarchy loses significance.

The tracing on images, necessarily required for such detailed study of bounding surface hierarchy, has been performed by combining HD and 4k panorama views and close-up images, always carefully verifying details.

DESCRIPTION

The sandstone bodies in the Font Nova sections incise and onlap blue grey bioturbated mudstone (Fig. 2B). The work includes both along-strike (Font Nova 1) and along dip (Font Nova 2) to the delta-slope transect. Because the Sandstone Unit B of Font Nova 2 correlates with the one which is exposed high in the cliff of the Font Nova 1 locality and is of poor quality, the authors decided to study the along-strike sandstone unit at the base of the cliff, which has very similar sedimentology and is only stratigraphically *ca* 20 m below the Sandstone Unit B in Font Nova 2. For the purpose of the present architectural and facies study of bedforms this approach was not regarded as a problem. The sedimentary logs of both localities are given in Fig. 4.

Font Nova 1

The sandstone unit at the base of the Font Nova 1 cliff locality (see Fig. 2B) truncates the underlying mudstones and thin bedded turbidites by means of a wide, some hundred metres across, V-shape fifth-order BS (Fig. 5A). Two fourth-order BS truncate a number of third-order BS to form channel fill storeys. Third order BS can be seen to envelop second-order BS delineating turbidite beds (Fig. 5C and D). The beds run concordant with the third-order BS pinching out in both directions. Third order BS form small, 10 to 20 m wide lenses mimicking festoon-like set boundaries. The BS hierarchy scheme in Fig. 5B sketches the Font Nova 1 outcrop.

At the sole of the thick sandstone bed just above the fifth-order BS are large grooves with a north-west – south-east orientation and various bounce and skip marks (Fig. 6A). Grain size strongly varies from very fine sand to coarse sand with fine pebbles (see log in Fig. 4). Amalgamation of sandstone beds is common and evident where internal truncations can be traced to localities with mudstone partings or BS truncating the amalgamated beds. Flute casts are found at third-order BS incisions and indicate north to north-west palaeocurrent directions (Fig. 6B). In particular along third-order BS and within bed set sequences there are conspicuous facies changes (Fig. 6C). Facies of the sandstone is often structureless just above the BS and at the deepest part of the incisions, yet lateral and upward facies are characterized often by three types of parallel bed stratification: (i) up to decimetre-thick stratifications with diffuse boundaries called crude-stratification (facies Tb3a); (ii) up to several centimetre-thick stratifications with sharp boundaries called spaced stratification (facies Tb3b); and (iii) up to 0.5 cm thick stratifications called planar stratification (facies Tb2 – see Fig. 3 for overview of here used turbidite facies types). The various stratification types can change from structureless to crude, and from spaced to planar going from the centre to the margin of the lens-shaped bed sets (Fig. 6C). Soft-sediment deformation in the form of load casts occurs often at the third-order BS

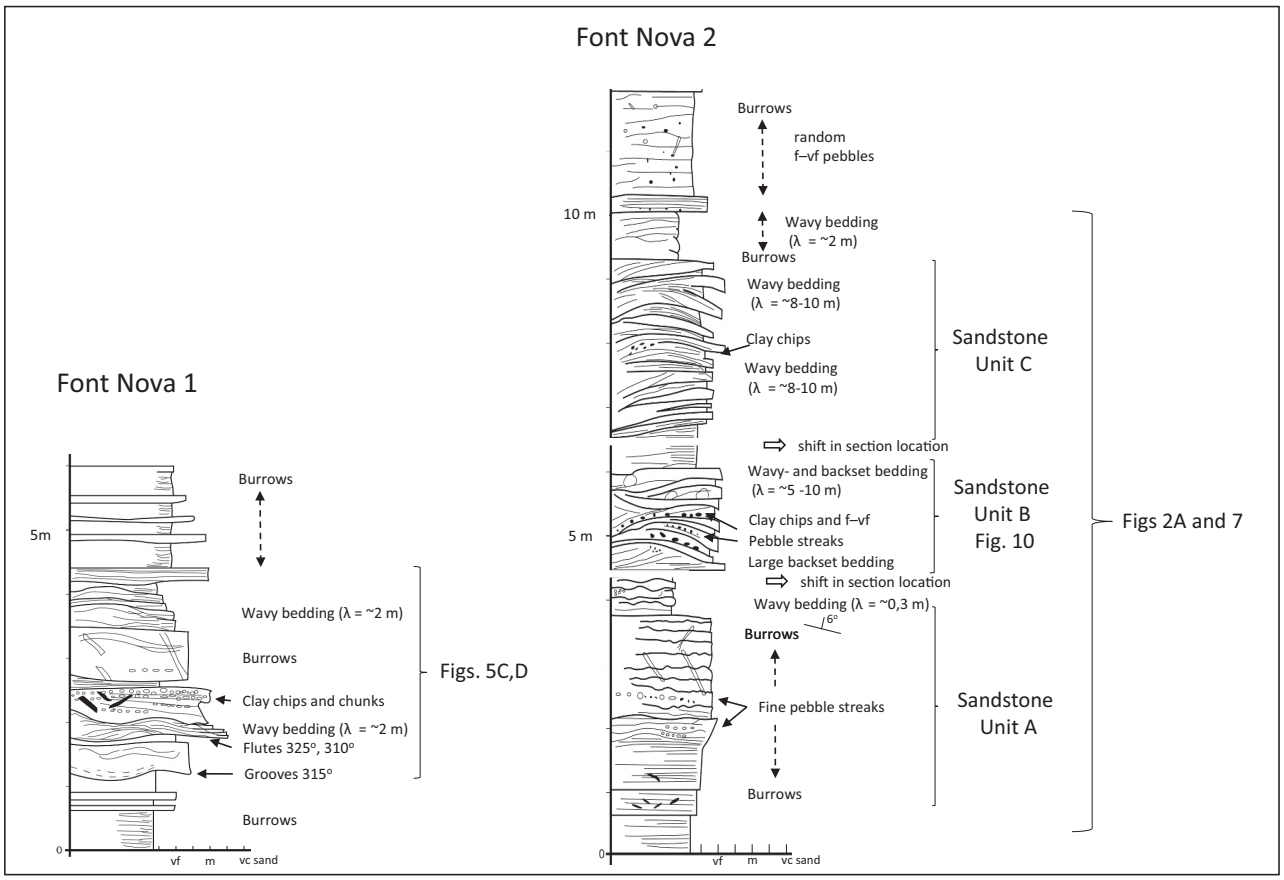

Fig. 4. Sedimentary logs of Font Nova 1 and 2 outcrops.

itself, and also within the thicker beds at grain-size breaks. Ripple cross-lamination has not been found in these beds. Just above the lower fourth-order BS several layers with abundant soft-sediment deformation, folded intraclasts and presence of abundant mudstone chips and folded sand clasts are found (Figs 5D and 6D).

Font Nova 2

The Font Nova 2 section provides sections parallel to palaeoflow with Sandstone Units A to C separated by blue grey mudstone (Figs 2B and 4).

Sandstone Unit A shows simple architecture of parallel beds with intervals of intensive burrowing and abundant tubes of *Rhyzocorallium*. Bed boundaries are diffuse and rare non-bioturbated facies shows structureless, lower-fine to upper very-fine sandstone layers a few centimetres thick with rare fine pebble streaks, with imbrication indicating flow direction to NNW. The sandstone layers are separated by mudstone drapes. Before the transition to the overlying Unit B there is a poorly bedded and bioturbated mudstone interval of a few decimetres thickness that weathers more easily than the underlying parallel bedded sandstone unit.

Sandstone Unit B has, in contrast to Unit A, a complex architecture, which is summarized in Fig. 7. The base of the unit is characterized by a sudden break in grain size from silty mudstone into fine-grained sandstone with fine pebbles. The grain-size break coincides with a truncation surface (fifth-order BS) on which backset beds onlap. The onlapping beds seem to form a continuous sub-unit showing few third-order BS making low angle truncations with beds (marked in transparent blue in Fig. 7B). Individual beds are enveloped by thin mudstone drapes, which show fine laminations and rare burrows (*Ophiomorpha*). The thickness of beds varies from several decimetres down to a few centimetres with no obvious trend in thickness variation. Grain size of the beds is fine to medium-grained sandstone alternating with layers of

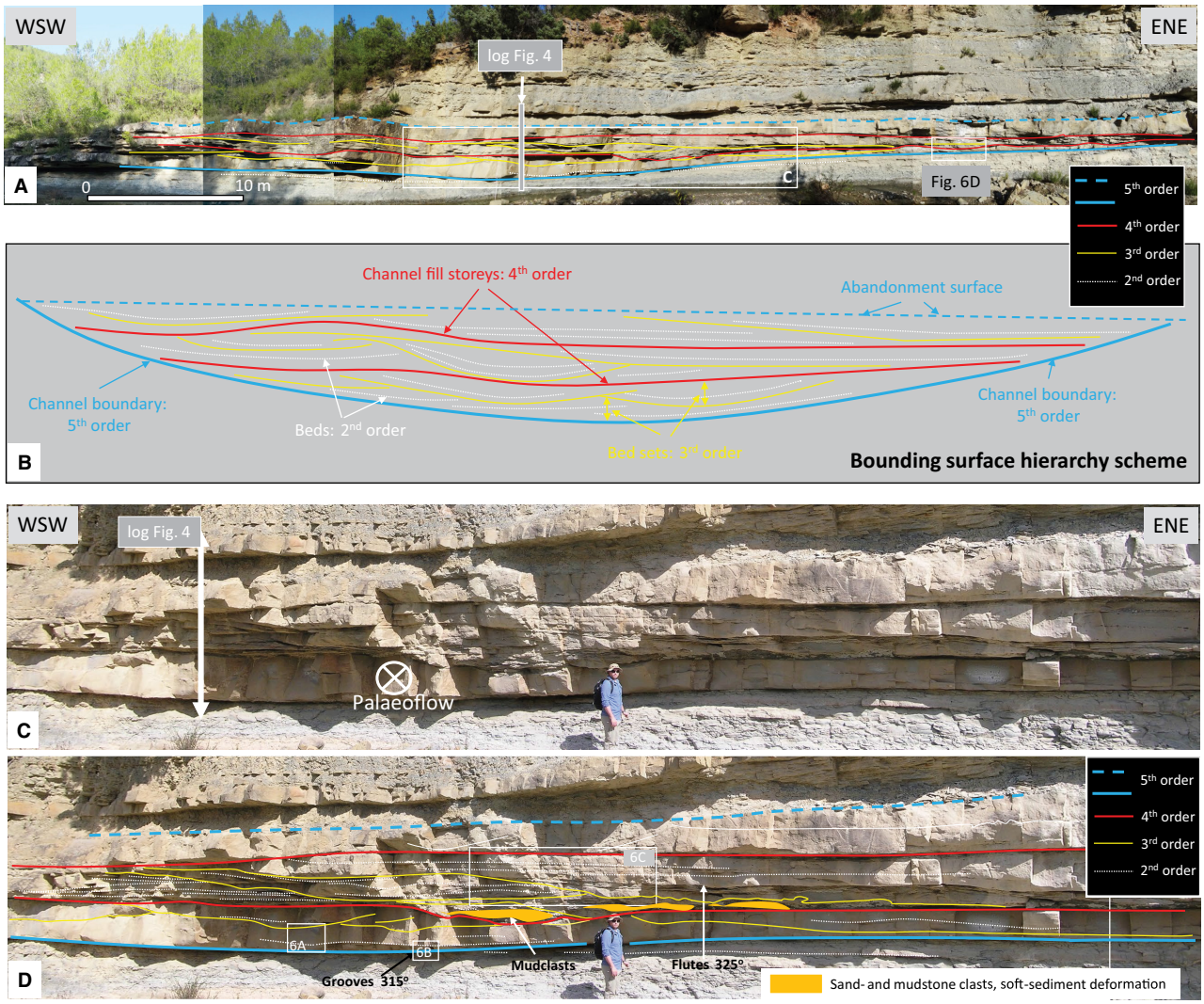

Fig. 5. (A) Cross-section about perpendicular to flow direction at Font Nova 1 locality (see Fig. 2). The solid coloured lines are truncation surfaces (bounding surfaces – BS). The fifth-order BS (solid blue line) marks the sharp, erosive base of the sandstone unit, which has a wide, V-shaped channel (chute) shape. Note the flat, lens-shaped geometries formed by the third-order bounding surfaces (solid yellow lines) truncating turbidite beds (see Fig. 5C). Third order BS are truncated by fourth-order BS (solid red lines) delineating channel-fill storeys. The top of the sandstone unit grades into mudstone and is indicated by a dashed blue line. Thickness of the sandstone unit is about 3 m. (B) Bounding surface hierarchy scheme which mimics the bounding surfaces in (A). Note the festoon-like third-order BS of the bed sets very similar to 3D cross-bedding. (C) and (D) Close-up of the inset in (A) showing the complex architecture of turbidite beds. Note the position of the grooves at the fifth-order bounding surface and the flutes at the third-order bounding surface. The dashed blue line at the top of the channel fill sequence is here assigned to be an abandonment (fifth-order) surface. Person for scale is *ca* 1.9 m tall.

coarse-grained sandstone and very fine to fine-pebble streaks. Facies of the beds consists of planar millimetre to centimetre stratification (Tb2), spaced stratification (Tb3b), and rare crude stratification (Tb3a) and structureless sandstones (Tb4). The transparent blue storey (Fig. 7B) is truncated over the full length of the outcrop by a fourth-order BS, which is irregularly undulating and associated with long and thick backset beds and intercalated mudstone matrix rich layers containing folded turbidite sandstone and mudstone intraclasts (Figs 8 to 10, 11B and 11C), either onlapping directly, or found close to the BS. The beds onlapping or directly overlying the lower fourth-order BS (transparent amber colour) are dominated by various traction carpet facies from structureless to crudely stratified (Tb3a) (Fig. 11A and C) and

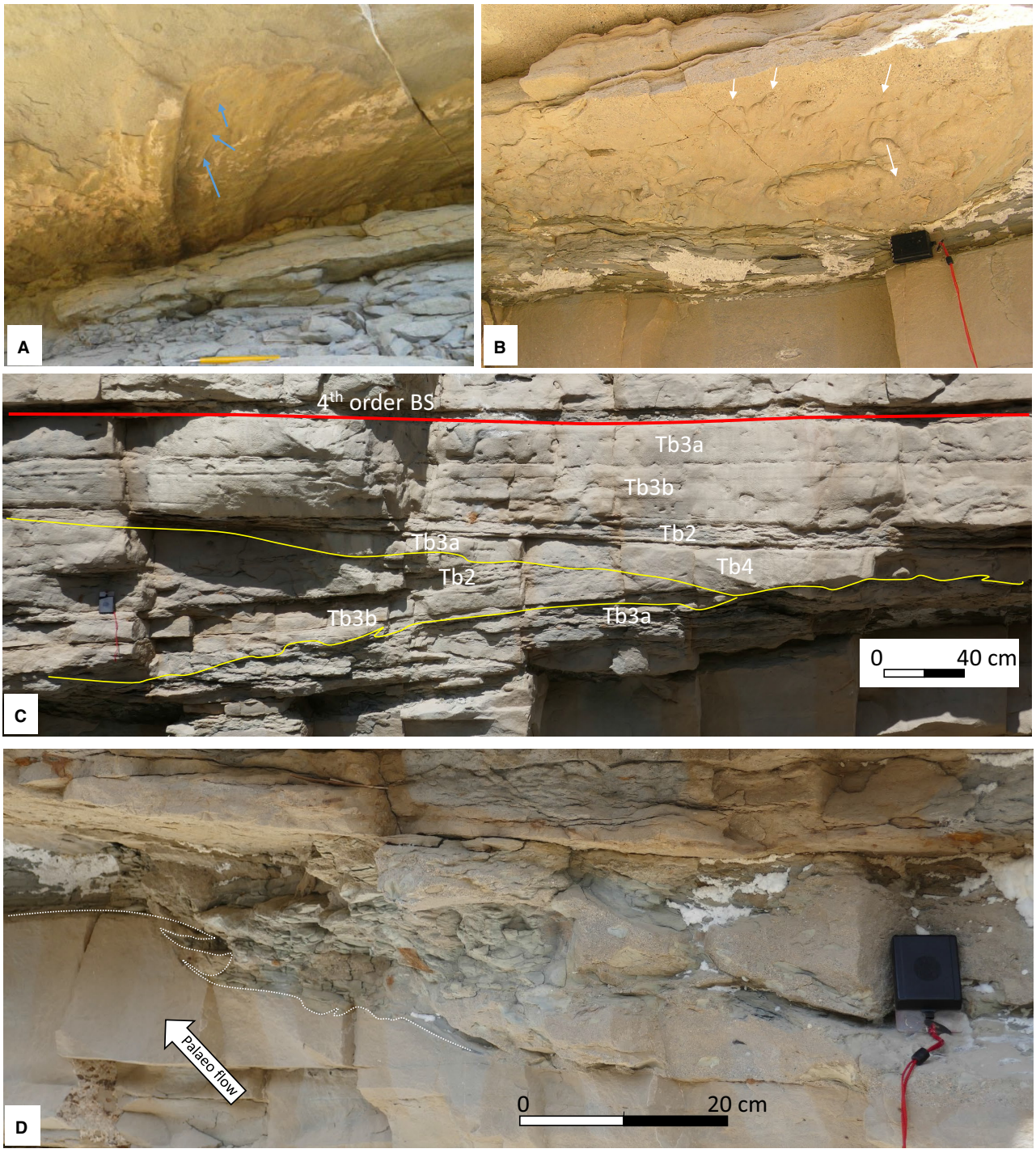

Fig. 6. Details of insets in Fig. 5A and D. (A) Grooves at the base of the bed at the fifth-order bounding surfaces (BS); pencil (*ca* 15 cm) for scale. (B) Flutes found at third-order bounding surfaces of 1.5 to 2.0 m wide scours; compass for scale (*ca* 10 cm) (C) Detailed view of facies types in bed sets enveloped by third-order BS (yellow solid lines). The various facies range from almost structureless (Tb4) and, occasionally, crude stratification in the centre to spaced (Tb3b) and planar (Tb2) stratification towards the margin of the bed set. Note soft-sediment deformation (flames and loadings) at the BS. (D) Soft sediment deformation in the top of the lowermost bed (locality at inset in Fig. 5A) above the fourth-order BS. Note the numerous mudstone and sandstone clasts, some of these being imbricated and others folded or otherwise deformed.

Fig. 7. The well exposed Sandstone Unit B is about 25 m above the Font Nova 1 channel incision (see Fig. 2A for its approximate position) and also represents channel fills but now seen in parallel flow section (palaeoflow to the NNW – to the left). The bounding surface (BS) hierarchy is verified by study of detailed images (Figs 8 to 10) and by sedimentary logs (white bars). The transparent colours highlight channel infill storeys and mark an inferred upward decrease in flow energy (see text). (B) Two times vertical scale exaggeration of (A) to show the consistent backset bedding in the various storeys. Note also the irregular preservation of time equivalent strata and the association of slumped strata (in orange) nearby the lower fourth-order bounding surface.

Fig. 8. Font Nova 2 locality (see Fig. 7). (A) and (B) Detailed bounding surface (BS) hierarchy study. Note the flat base and upslope onlapping large, low-angle backset beds of second-order (white dotted lines). The beds are truncated by third-order BS (yellow), which in turn are truncated by a fourth-order BS (red lines) that can be traced throughout the exposed sandstone unit. Again, backset beds truncated by third-order BS cover the fourth-order BS. The transparent orange colour marks a level of reworked strata. (C) Close up view of the reworked segment just above the fourth-order (red) BS, showing large sandstone clasts (some of which folded) in a mudstone matrix. The second to fifth BS hierarchy is illustrated in detail. Vertical bar gives approximate scale. Note the thin–thick bedded sandstone unit at the top with intercalated mudstone-rich and burrowed intervals marking gradual abandonment.

contain structureless sandstone with rare pebble layers at their top that can be assigned to facies Tb4 (see Fig. 3). Ripple cross-lamination has not been found. Current indicators are rare, with the best measurements from imbricated pebble and mudstone chips indicating north-west to north palaeoflow (for example, Fig. 11D).

The transparent amber coloured storey (Fig. 7B) is truncated by a second fourth-order BS that is undulating with a 15 to 20 m wavelength. This boundary is draped by upslope climbing beds of similar wavelengths locally truncated by third-order BS (yellow transparent colour in Fig. 7B). Beds are predominantly characterized by crude and spaced stratification of type Tb4, Tb3a, Tb3b and Tb2. These deposits are again truncated by another fourth-order BS with wavelengths of 30 to 50 m and draped by thinner beds than in the previous subunit (blue transparent colour in Fig. 7B). Facies shows predominantly planar and plane bed laminations (Tb2 and Tb1) with some spaced and crudely stratified (Tb3a and Tb3b) facies in thicker beds (Fig. 12C). Rare ripple cross-lamination is found within intercalated mud-rich and burrowed intervals (Fig. 8C). Good palaeoflow indicators in the here found facies were strikingly rare, yet present in the form of imbricated clay chips, imbricated pebbles found in rare pebble layers, and palaeoslope estimates from folded strata. Good measurements are too few to plot them in a rose diagram. The overall northward progradation of the delta clinoforms, however, is in accordance with the rare-measured palaeoflow directions.

In the overview picture with a two times vertical exaggeration (Fig. 7B), the upslope stacking of beds in Sandstone Unit B is most evident: At first the blue unit develops, then the orange unit followed by the yellow and the pale blue unit that can all be traced for significant distance upslope. The beds of the yellow and pale blue unit show upslope migration. The coloured units show that preservation of strata varies significantly. The top of the sandstone unit is not well-defined and non-erosive, and is marked with a dashed blue (fifth-order) line (Fig. 7). The overlying mudstone unit is truncated by Sandstone Unit C (see also Fig. 4).

Sandstone Unit C has very similar architecture and facies as Sandstone Unit B (Fig. 12, see inset Fig. 2C for locality) and is not described in the same detail. Large backsets are also truncated by wavy, third-order truncation surfaces draped by upslope climbing thin and thick beds, whose architecture and facies dominate the unit in downslope direction. Individual thin beds can be found draping the entire third-order wavy BS and then dominated by Tb1 and possibly Tc facies (the latter only judged by the wrinkled architecture of first-order and second-order BS). Interestingly, the third-order BS delineate flat, dome-shaped 'laminae' sets. The thick beds are found predominantly as backset beds pinching in upslope direction. These show a variety of stratifications Tb3a, Tb3b and Tb2 (Fig. 12C).

INTERPRETATION

Font Nova 1

Architecture

The cross-section in the Font Nova 1 outcrop shows a large, V-shaped truncation into parallel bedded bioturbated mudstone at the base of the sandstone unit, which suggests a channel boundary. A channel interpretation is also in accordance with the bounding surface order: fourth-order BS onlap the channel margin (fifth-order BS), delineating channel storeys (Sprague *et al.*, 2005). The channel width is limited to some hundred metres, and groove orientation and north to north-west flute directions reconcile with the general progradation direction of the delta clinoforms (Fig. 2B). It thus points to channels formed on the delta slope. Also, the *Rhyzocorallium* ichnofacies reconciles with relatively high energy (turbulent), oxygenated settings of a delta slope (e.g. Eagar *et al.*, 1985) and

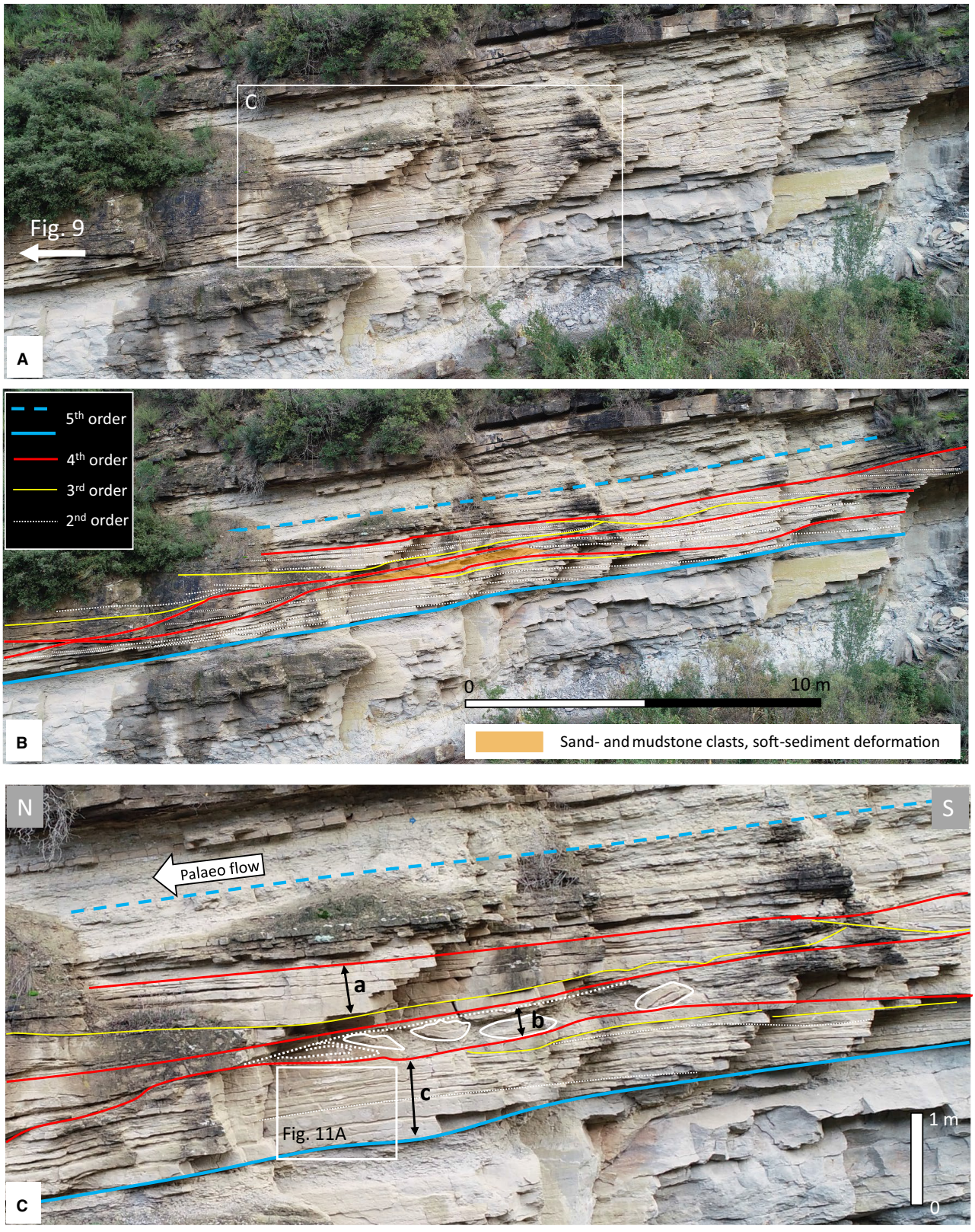

the absence of wave rippled beds and the total measured thickness of the prograding delta sequence indicate water depths below storm wave base.

The third-order BS (set boundaries) form a festoon structure, comparable to set-boundaries of cross-bedding, that is cut perpendicular to the palaeocurrent direction (Fig. 5). The third-order BS envelop some tens of metres wide, lens-shaped bed sets, the beds themselves deposited by various types of sediment flows as shown by their different facies (discussed below). The mudstone partings in between the individual sandstone beds indicate that deposition must have occurred by many separate sediment flow events. The authors infer that this type of architecture represents large three-dimensional (3D) bedforms similar to those observed on the slope and at the base of slope of the modern Squamish deep-water delta (British Columbia; e.g. Hughes Clarke, 2016; Clare *et al.*, 2016; Vendettuoli *et al.*, 2019). Because the type of bedform is best determined from flow parallel sections (e.g. Alexander *et al.*, 2001; MacDonald *et al.*, 2009; Cartigny *et al.*, 2014), the analysis will be done when interpreting the Font Nova 2 outcrop.

Facies

Most beds are dominated by various types of stratification of facies Tb4, Tb3a, Tb3b and Tb2 (see Fig. 3) all interpreted to be produced by traction carpets, which are commonly ascribed to high-density turbidity currents (Lowe, 1982; Baas *et al.*, 2004; Leclair & Arnott, 2005; Talling *et al.*, 2012; Cartigny *et al.*, 2013). Such flows are stratified with a dense basal layer that is interacting with the substrate and its low-density top layer. The basal layer is driven by its own density and may also be driven by the overriding low-density upper part of the flow if the

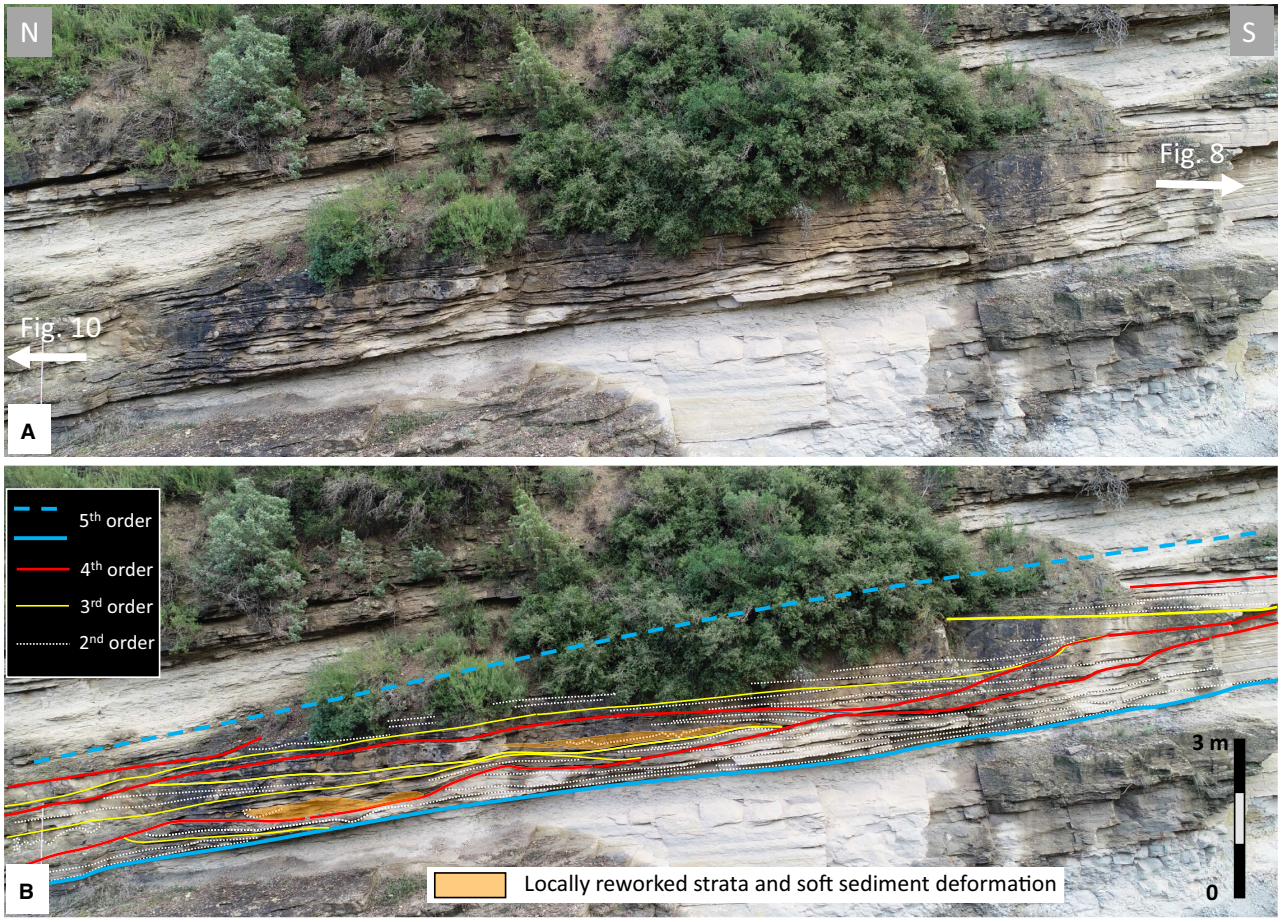

Fig. 9. (A) and (B) Down flow continuation of Sandstone Unit B from Fig. 8. Note the position of two beds showing deformation (orange) with respect to the fourth-order bounding surface (BS). Vertical bar gives approximate scale.

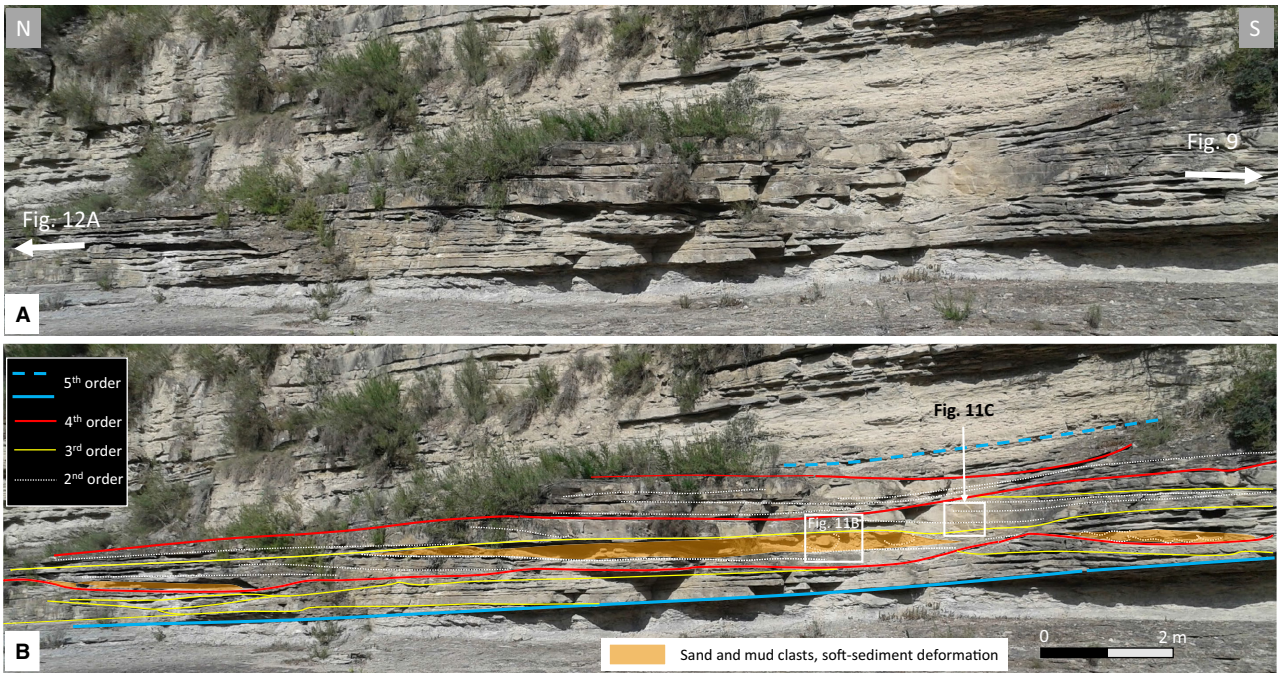

Fig. 10. (A) and (B) Down flow continuation of Sandstone Unit B from Fig. 9. Note continuation of the lowermost subunit with gentle backset bedding and the presence of three zones with reworked strata above the fourth-order bounding surface (BS). Note that backset beds onlap third-order and fourth-order BS. Horizontal bar gives approximate scale.

latter is faster (e.g. Postma *et al.*, 1988). A diagnostic criterion for a faster flowing overriding low-density turbidity current is poorly stratified Tb4 facies topped by a layer of imbricated, outsized clast, such as present in the beds above the first fourth-order BS. Preservation of the deposits of high-density, stratified turbulent underflows on delta slopes is not regarded as uncommon (e.g. Mutti *et al.*, 1996, 2003; Plink-Björklund & Steel, 2004; Petter & Steel, 2006; Zavala & Arcuri, 2006; Bhattacharya & Maceachern, 2009). They have been observed to occur on the modern Squamish fjord-head delta by daily monitoring with acoustic profilers. Real time videos show how the dense part of stratified hyperpycnal flows with basal layers of about 1 to 2 m thick cause the upslope migration of cyclic step bedforms (Hughes Clarke, 2016).

The layers that show deformation, flames, clay chips and deformed sand clasts above the fourth-order BS point to slumping on a rather small scale (up to several metres). Their origin is easier to understand in parallel flow sections, i.e. Font Nova 2 and is dealt with there.

Grooves at the fourth-order BS of Font Nova 1 locality and flutes at third-order BS are both covered by Tb3a and Tb3b traction carpet deposits (Fig. 6), and thus were likely formed during deposition of the basal layer. Peakall *et al.* (2020) recently pointed out that the origin of grooves and flutes must be different: grooves are linear structures not showing evidence for rolling or bouncing of clay clasts (e.g. Dżułyński & Sanders, 1962), and flutes are spoon-shaped moulds, likely to be produced by flow separation (Allen, 1968, 1971). Hence for grooves it must mean that the basal sediment layer was sufficiently rigid (dense) to keep the clasts in position and for the formation of flutes the basal layer must have been sufficiently dilute to allow internal flow separation to occur. Although flow characteristics of the basal layer are still not fully understood, experiments by Postma *et al.* (1988) show a pseudo-laminar flowing basal layer that is unlikely to be capable of holding the clasts sufficiently long in position to produce the grooves. Interestingly, however, are recent turbidity flow measurements in the Monterey Canyon by Paull *et al.* (2018), which show a basal layer that outruns the overlying turbidity current. If such a basal layer would slide over the slope by hydro-planing, thus acting as a sliding rigid body, it would be capable of holding

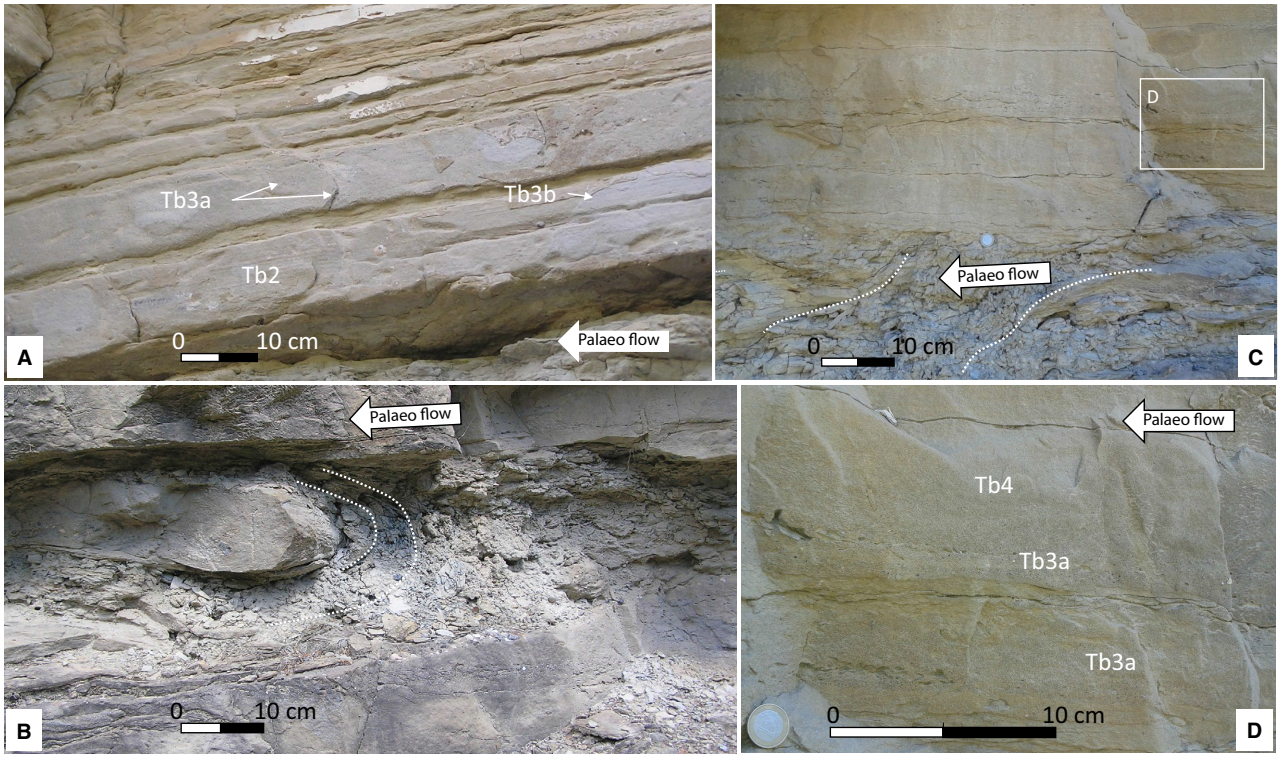

Fig. 11. (A) Detail of the backset beds (see inset Fig. 8C) enveloped by fine-grained intervals. The lowermost bed shows spaced stratifications type Tb3b and Tb2 (white arrow), poor grading and virtually structureless non-graded fine to medium sand size. (B) Reworked strata (interpreted as local slumps) showing folded sandstone clast and mudstone layers (indicated by white dotted lines) on locally eroded strata (locality indicated by inset in Fig. 10B). (C) Beds directly overlying the folded sediment layer shown in (B) (see inset Fig. 10B). (D) Detail of the beds at the inset shown in (C). Note the structureless (Tb4) to crudely stratified (Tb3a) fine to medium-grained sandstone containing streaks of imbricated mudstone-chips (indicating northerly flow direction here to the left).

mud clasts in position. In this way the basal layer was able to produce grooves before it was remoulded and transformed into a stratified flow of which the basal part is of high-concentration exhibiting quasi-laminar flow behaviour that produces the overlying traction carpet deposits. If the here inferred flow characteristics for grooves would hold, then it means that the flow that initiated the channel incision would have different flow characteristics than the flows that shaped the bedforms higher up in the same unit. The initiation of the channel might then be related to a catastrophic flow event, while the backfill would relate to 'normal' sustained flow events. The importance of catastrophic versus sustained turbidite events for bedform architecture and preservation in the channel–lobe-transition-zone (CLTZ) was highlighted recently by Vendettuoli *et al.* (2019) based on data of the modern Squamish fjordhead delta. The catastrophic events have been related to delta-lip collapse, while the sustaining flow events were generated by extra river discharge from spring meltwaters (see also Clare *et al.*, 2016).

Font Nova 2

Architecture

The simple planar architecture and thoroughly bioturbated beds of Sandstone Unit A in conjunction with their Tb3a, Tb3b and Tb2 primary structures suggest deposition by sustained subcritical hyper-concentrated flows (Postma & Cartigny, 2014) possibly in a lobe or inter slope-channel setting.

In Sandstone Unit B the fourth-order BS delineate four storeys (shown with a different colour in Fig. 7B). All stories show beds onlapping the fourth-order BS thus forming back sets enveloped by third-order BS. The flat lens-shaped architecture of third-order BS in Sandstone Units B and C points to tens of metres

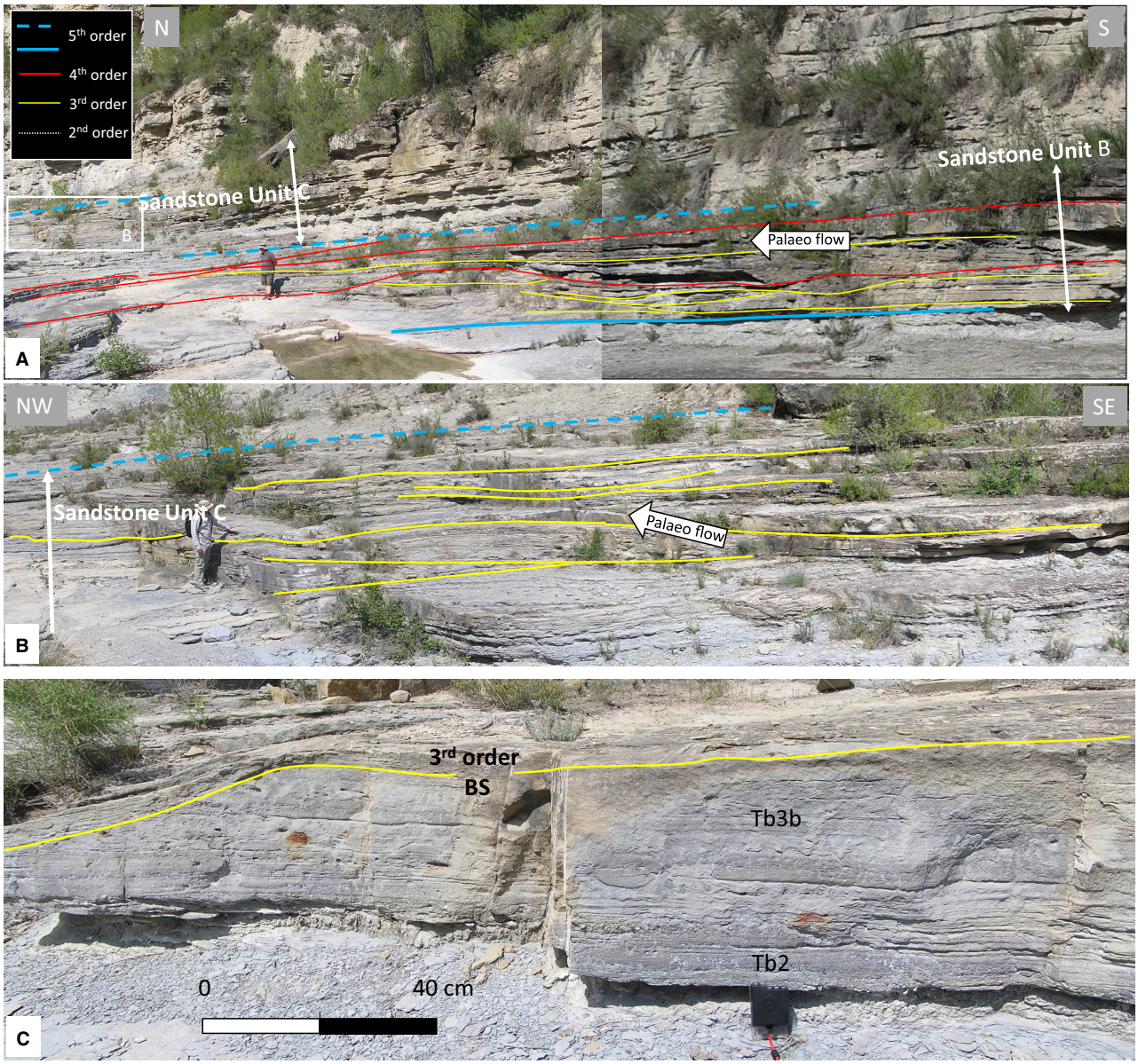

Fig. 12. (A) Most down slope view on Sandstone Units B and C. The view becomes almost perpendicular palaeoflow to the left of the geologist (*ca* 1.8 m tall). Note that truncations imply strong three-dimensionality of the bounding surface (BS). The top two wavy fourth-order BS are converging and draped by thin beds similar to those seen in (B). (B) Wavy third-order BS (yellow). The units are dome-shaped implying three-dimensional morphology of bedforms. The flat lens-shaped bed sets with thin beds pinching out in all directions are indicative for antidunes (see Fig. 13). (C) Detail of beds showing sharp third-order BS truncating thin beds that form the antidune. The thin beds are pervasively stratified, mainly with planar stratifications (Tb2) and spaced stratifications (Tb3b), and show intercalated fine pebble and granule layers. Cross-bedding is absent here.

large three-dimensional bedforms similar to those inferred from Font Nova 1 outcrop but here in flow parallel section. This clearly points to 3D bedforms (compare Figs 5 and 7). Because backset development is characteristic for both cyclic step, chute and pool and antidune bedforms (e.g. Alexander *et al.*, 2001; Cartigny *et al.*, 2014; Postma & Cartigny, 2014; Fedele *et al.*, 2016), additional criteria are needed to determine the type of bedform.

Architectural criteria for determining supercritical-flow bedforms

The architectural differences between cyclic step, chute and pool and antidune bedforms have been studied from flow-parallel video

images of runs in open channel flow experiments (e.g. Alexander *et al.*, 2001; Cartigny *et al.*, 2014). Careful tracing of the moving bed surface against the glass wall of the flume in conjunction with an algorithm that mimicked different aggradation rates visualized resultant architecture (Cartigny *et al.*, 2014), which is summarized in Fig. 13. The cyclic step architecture is fairly simple, although variations on the basis of net aggradation and erosion exist (Slootman & Cartigny, 2020). Backset beds formed on the stoss side of cyclic step and chute and pool bedforms are straight and relatively thick where these onlap the fourth-order BS in the blue and orange storeys (Figs 7B, 8C, 9 and 13). The upslope moving hydraulic jump zone is characterized by soft-sediment deformation, slumping of the lee-side (e.g. Cartigny *et al.*, 2014) and hindered settling forming coarse-tail graded (Ta) beds (Postma *et al.*, 2009). Such architecture contrasts with 3D antidunes, which are observed to thin in all directions (Fig. 12). For the chute and pool bedform, the degree of preservation of the backset beds is not only determined by the aggradation rate but also by the erosion depth of the co-existing up-slope migrating antidune bedforms (Cartigny *et al.*, 2014).

The experiments by Alexander *et al.* (2001) and Cartigny *et al.* (2014) are using shallow water flows, and for particulate turbidity currents such experiments are rare. The only available experimental data is on basis of supercritical-density currents (salt solutions) and a few reported dilute turbidity currents (Fedele, 2002; Sequeiros *et al.*, 2010) that move over a loose grain bed. Here, the view is taken that laboratory results obtained by saline density currents can be extended to muddy turbidity currents moving over a mobile bed of grains as long as analogous conditions of the bed shear stress (Shields number) and densimetric Froude number are maintained. These experiments provide useful data that confirm the formation of cyclic steps on internally formed deltas (Spinewine *et al.*, 2009) and even cover the entire spectrum of bedforms created by saline underflows from antidunes to cyclic steps (Fedele *et al.*, 2016, fig. 19), although observations of long-wavelength upstream-migrating antidunes transitioning into upper-plane bed at

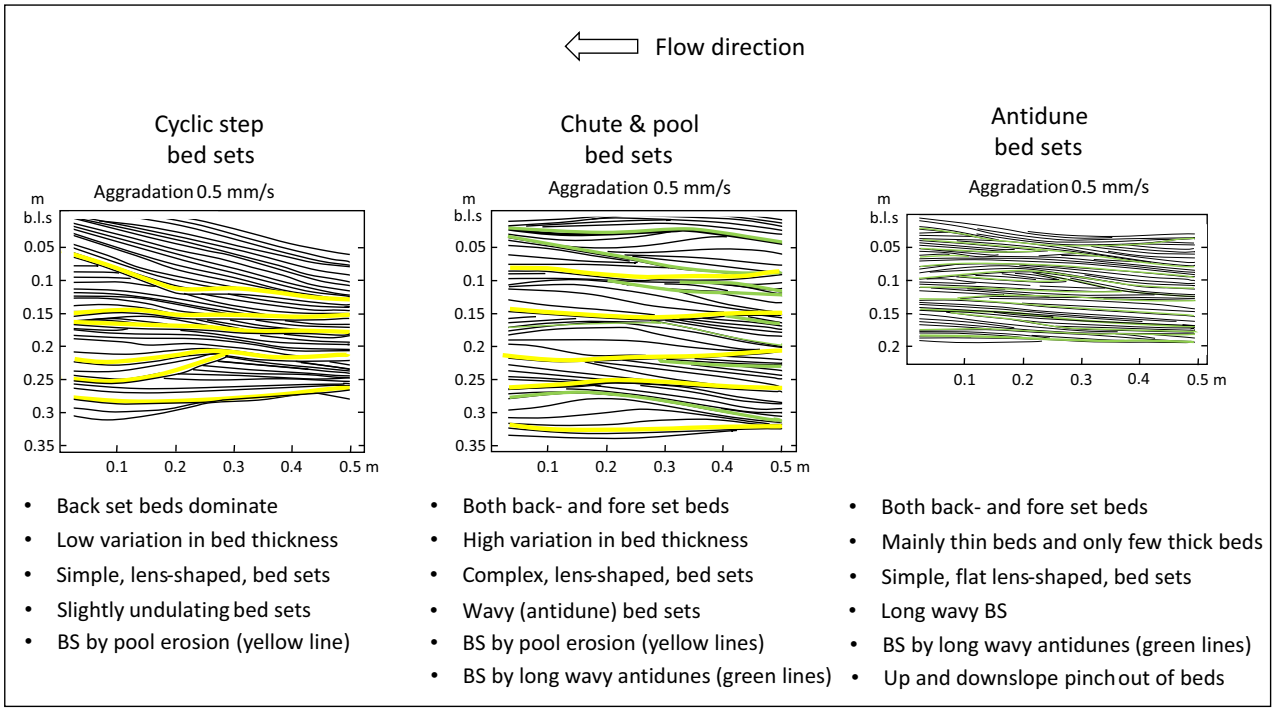

Fig. 13. Strata formation by cyclic step, chute and pool and antidune bedforms studied from video images of unidirectional supercritical-flow flume experiments by Cartigny *et al.* (2014). Here the solid yellow lines are set boundaries produced by upslope migration of cyclic step and chute and pool bedforms and the black solid lines represent the laminae. Green solid lines mark set boundaries produced by upslope migrating antidunes.

densimetric Froude numbers higher than two are not known from modern environments. Hence, criteria for variation in bedform dynamics must come from recognizing: (i) bounding surface hierarchy; (ii) facies; and (iii) flow directions.

Hence, in line with the experimental data discussed above, it is inferred that the simple and straight backset beds onlapping the fifth-order BS (blue transparent unit in Fig. 7) may thus be related to cyclic step bedforms and the rare third-order BS in this unit indicating some undulation of the bedform in the third dimension. The backset beds above the fourth-order BS truncating the basal transparent blue subunit may be related to the upslope migration of chute and pool bedforms or mouthbar with a chute and pool structure (see also Postma *et al.*, 2016), because its backset beds are truncated by wavy, upslope-climbing beds of 15 to 20 m wavelength interpreted as antidunes (Alexander *et al.*, 2001; Cartigny *et al.*, 2014; Fedele *et al.*, 2016).

Bedform facies

Sedimentary facies in the Sandstone Units B and C are very similar to that found in Font Nova 1 outcrop and are dominated by stratified sandstone of facies Tb3a, Tb3b and Tb2, formed by traction carpets below high density turbidity currents (e.g. Postma *et al.*, 1988; Sohn, 1997; Cartigny *et al.*, 2013). The layers with abundant localized soft-sediment deformation, large mud clasts and deformed sandstone clasts are interpreted as small, local slumps (marked in Figs 7, 8 and 11). These slump deposits are covered by Tb4 and Tb3 facies near and at the fourth-order BS (Fig. 11C) and onlap the fourth-order BS. The onlap suggests that the fourth-order BS represents the deepest part of the bedform trough and its wobbly appearance then must reflect the variation in erosion depth that is inherent with a 3D bedform. Hence, the local slumps must stem from instability of the lee face of the bedform. Such instability of the lee side of migrating supercritical-flow bedforms is observed in the experiments of Cartigny *et al.* (2014). Hence, the two stacked fourth-order BS, the lower one with large onlapping backset beds and the upper one with in-phase draping turbidite beds, display similarities with the architecture of an upslope migrating chute and pool bedform found in experiments with open-channel flows (Fig. 13; Alexander *et al.*, 2001; MacDonald *et al.*, 2009; Cartigny *et al.*, 2014).

The flow dynamics for the bedforms in Font Nova 2 can now be reconstructed on the basis of antidune wavelength and facies characteristics. Thickness of the basal layer (d) can be assessed by using the observed antidune wavelength (L, ranging from 15 to 20 m and 30 to 50 m – see Fig. 7) in the formula $d = L \times \rho_1/[2 \times \pi \times (\rho_1 + \rho_2)]$ and where ρ_2 is the density of the flow, and ρ_1 the density of the ambient fluid empirically found by Hand (1974). If the density of the ambient seawater is assumed to be 1035 kg m^{-3}, and inferring a density of the basal part of 1200 to 1400 kg m^{-3} (concurring with initial grain concentration of the flow C *ca* 0.10 and 0.30 for Tb3 type traction carpets following Cartigny *et al.* (2013), the basal layer thickness would be of the order of *ca* 1 m. In addition, empirically-derived relations between antidune wavelength and flow thickness, as function of grain size and Froude number for stable antidunes (see Fedele *et al.*, 2016) also predict similar ranges for (main) flow thickness (for example, d/L between 15 and 22 for these observed grain sizes). Interestingly, similar basal layer thicknesses where monitored to shape the cyclic step bedforms on the Squamish delta slope (Hughes Clarke, 2016).

The top of Sandstone Unit B is again truncated by a fourth-order BS, but here draped by long wavy antidunes of 40 to 50 m wavelength. This would suggest a flow thickness of *ca* 3 m, which is presumably the thickness of a low-density, non-stratified flow, which reconciles with the thin beds, the Tb2 and Tb1 and rare Tc facies and intercalated burrowed mudstone layers and gradual transition into mudstones separating Units B and C.

In Sandstone Units B and C the chute and pool bedform structure evolves downslope into antidunes (Figs 2 and 12). The significance of the downslope increase in antidunes is further discussed below. It is further noted that the dome-shaped set boundaries (third-order BS in Unit C) provide evidence for a three-dimensional bedform structure thus implying undulatory antidune crests.

DISCUSSION

Experiments demonstrate stable existence fields for antidunes and cyclic steps, but suggest that chute and pool bedforms are potentially unstable (Alexander *et al.*, 2001; Cartigny *et al.*, 2014), with little chance to be preserved in the record (see also Slootman *et al.*, 2019a), yet their

potential for preservation is demonstrated by the here described sandstone units. The well-monitored Squamish deepwater delta shows clearly that supercritical-flow bedform architecture is not only governed by their erratic preservation, but much is also due to variation in discharge of the density underflows that produce these bedforms (Clare *et al.*, 2016; Hage *et al.*, 2018; Vendettuoli *et al.*, 2019). Particularly, the CLTZ, which is found near the base of slope of the Squamish delta clinoform shows a variety of bedforms with rapidly changing morphology and preservation over very short distances (few hundreds of metres). It also opens the possibility that the here described chute and pool bedform backfilling the slope channel is a consequence of a solitary hydraulic jump migrating upslope, thus being related to a mouthbar in the channel–lobe transition zone as invoked by Postma *et al.* (2016) for slightly older deposits in the same delta wedge (locality 1 in Fig. 1C). Thus, instead of interpreting the Sandstone Units B and C structures being the result of chute and pool type bedforms, can a mouthbar origin be inferred on basis of the here presented observations? In the following discussion this problem is addressed and the stacking of the bedform structures in Sandstone Unit B is evaluated.

Mouthbar in the channel–lobe transition zone

The existence of a solitary hydraulic jump moving upslope in a CLTZ was investigated by experimental studies of Hoyal & Sheets (2009) and Hamilton *et al.* (2015, 2017). The studies showed: (i) that erosive channels are formed by supercritical flows that feed and prograde the lobe at the base of slope; and (ii) that a hydraulic jump, which is triggered by the lobe obstruction, heralds the backfilling of the channel and the development of backset bedding upslope of the formed mouthbar. Hamilton *et al.* (2017) found a positive relationship between channel hydraulics and lobe element thickness of supercritical flows. More specifically, these authors argue that the sequent depth (ratio of incoming flow depth and flow depth after the jump) is an important factor between in-channel densimetric Froude number and lobe thickness. In simple terms, the flow has to increase its thickness to overcome the obstruction. Supercritical flows do this by means of the hydraulic jump, and subcritical flows by increasing the backwater depth. Fluctuations in flow discharge and different discharges in subsequent events may similarly have important impacts on lobe element thickness and the triggering of a mouthbar related hydraulic jump (Postma & Kleverlaan, 2018). The authors hypothesize here that high discharge flows might develop thick basal layers that aggrade the lobe so that they become large obstructions to lower discharge flows, possibly inducing hydraulic choke and the generation of internal hydraulic jumps. Once the hydraulic jump scoured the substrate, the sequent depth is increased and the hydraulic jump zone will remain, gradually moving upslope leaving deposits akin to cyclic steps (see Postma & Kleverlaan, 2018) and possibly chutes and pools. Strictly speaking such deposits must be classified as upslope growing mouthbars, which may display all of the characteristics of a chute and pool or cyclic step bedform in cross-section, but which have quite different geometries and spatial extent.

The architecture of Sandstone Unit B (Fig. 7) displays a few notable features including the very irregular fourth-order BS on which backset beds onlap and the domination of antidunes downslope of the point where the lower fourth-order BS flattens. The occurrence of both features can be explained by geometrical modelling of a chute and pool form that migrates upslope starting from a deep scour (Fig. 14A). Assuming the first deep incision in the fourth-order BS to be caused by a strong hydraulic jump, as evidenced by backset beds associated with local slumps, an idealized chute and pool profile can be migrated upslope along the irregular BS. The exercise indicates continued re-shaping of upslope migrating antidunes, upslope migration of backset beds and truncation features as observed in the upper three storeys of Sandstone Unit B (Fig. 7), the backset bed and antidune preservation being related to the bumps in the pool-related scour. Figure 14B also shows a striking similarity between modelled and observed antidune erosion depth (brown-yellow dashed line in Fig. 14B) as related to the irregular fourth-order BS on which the backset beds onlap.

However, inferring from this simple geometrical modelling exercise that the observed bedform structures are related to a solitary, upslope migrating hydraulic jump zone in the CLTZ, does this reconcile with other observed phenomena in Font Nova 1 and 2? Although the lobe environment is not very well constrained here, its presence may be suggested by the planar beds in Font Nova 2 (Sandstone Unit A), and the antidune fields in the most downslope parts of Sandstone Units B and C. Furthermore, the vertical sequence in Sandstone Unit B shows a

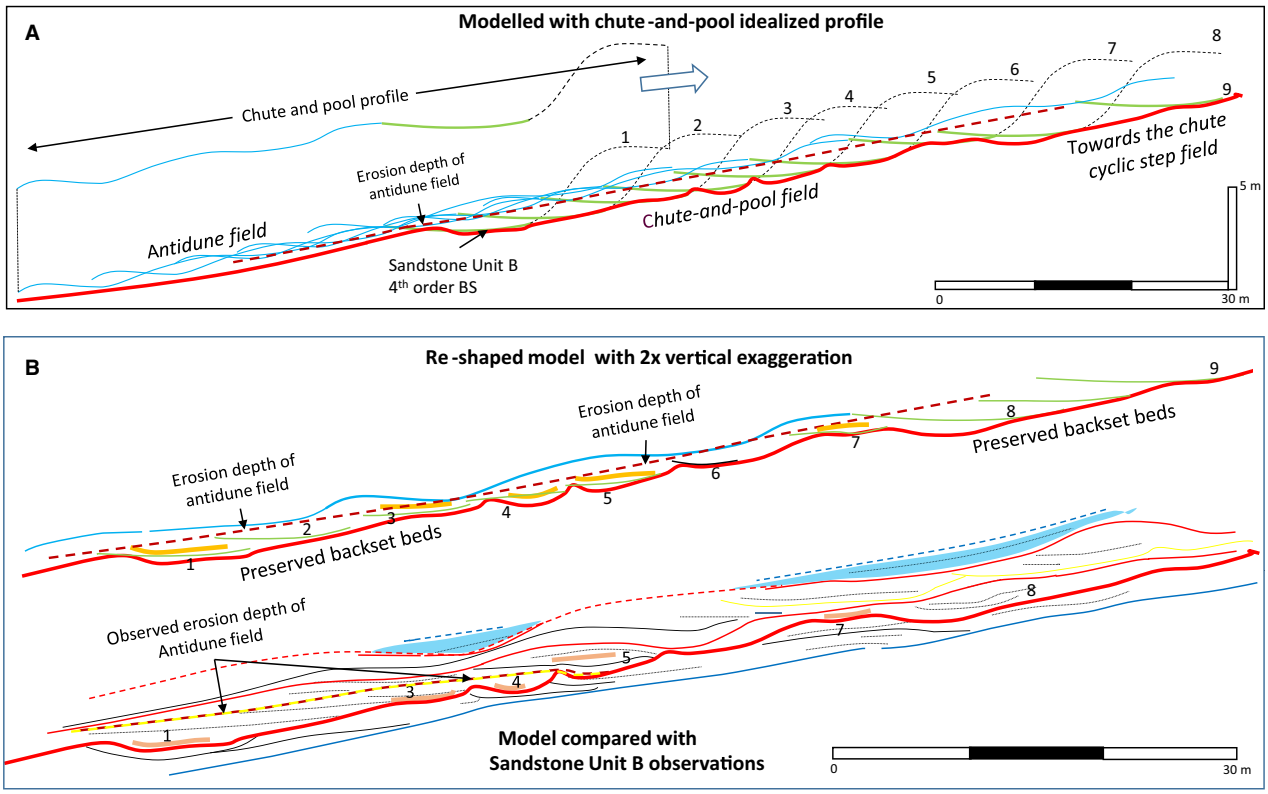

Fig. 14. A. Geometrical modelling of a chute and pool structure migrating upslope. Shape of the bedform is based on observed antidune wavelength and height (blue line segment) and backset bed inclination (green line segment) in Sandstone Unit B. The geometrical modelling allows first order assessment of preserved bedform architecture by migrating the profile along the observed fourth-order bounding surface (BS) of Sandstone Unit B. Upslope migration is chosen at the point of observed strong erosion (see Fig. 12). Successive timelines are dashed and indicated by numbers '1' to '9'. (B) Clean-up of the model shows outcrop conspicuous features including backset beds associated with slump deposits (thick orange lines) and fourth-order wavy antidune BS (blue line), which can now be compared with the outcrop simplified in the bottom profile. Note that the fourth-order wavy surface truncating the backset beds would correspond with dotted time line 8.

backfill development: backset beds possibly related to cyclic step bedforms onlap the fifth-order BS, and are truncated by the chute and pool (mouthbar) structure and covered by long-wave antidunes that seem to herald the gradual abandonment of the chute. Hence, there is no repetition of an irregular fourth-order BS that would point to aggrading bedforms (compare with aggrading bedforms in Fig. 13). The close proximity of the antidune field with the planar bedded beds of inferred lobe deposits would favour a base of slope setting with very small lobes (Fig. 15). Hence, the inferred size of the CLTZ is rather in the order of a few hundred metres than a few kilometres, and thus much smaller than the CLTZ on the modern slope of for example the Golo Fan (e.g. Deptuck *et al.*, 2008) and not matching the lobe development in small radius fans as discussed by Postma & Kleverlaan (2018). As suggested earlier, the here described units would best match the CLTZ at the base of slope of Squamish delta (e.g. Vendettuoli *et al.*, 2019, fig. 2), where the base of the chute is characterized by erosion, while aggradation of the supercritical-flow bedforms in this trajectory is continuously subject to significant change in discharge due to delta lip collapses occurring intermittently with river flood generated underflows (Clare *et al.*, 2016). Converging fourth-order BS (Fig. 12) found in the studied examples herein are illustrative for an extremely discontinuous time record in the sections.

Final note on bounding surface hierarchy approach

To understand complex architectural styles in the rock record, the bounding surface hierarchy

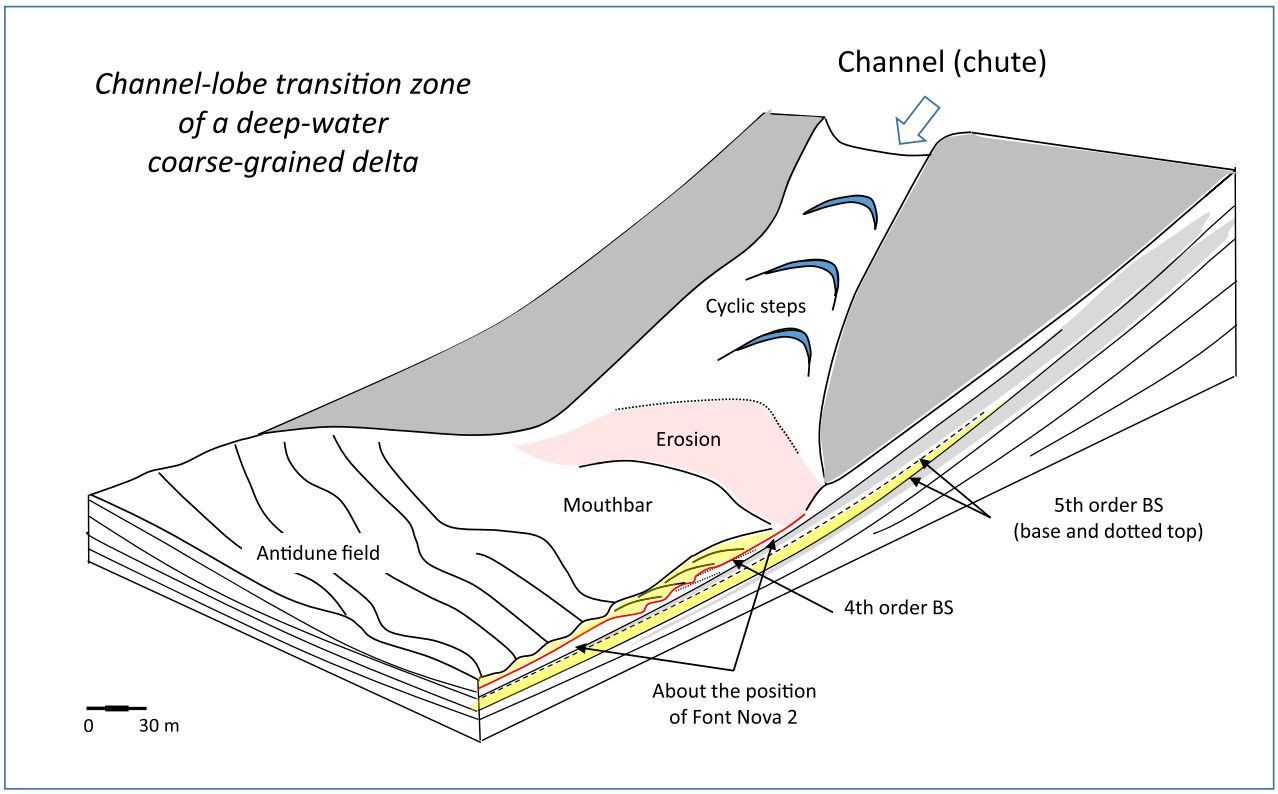

Fig. 15. Summary diagram showing an antidune field at the time of upslope migration of the mouthbar in the channel–lobe transition zone (CLTZ) at the base of slope of a prograding deep-water delta (inspired by the study of the CLTZ of Vendettuoli *et al.*, 2019).

proved to be important. It focussed the descriptions here of the large, near outcrop-scale bedforms significantly by establishing set boundaries. The establishment of channel storey (fourth-order) and bed set boundaries (third-order) were crucial for determining the type of bedform. The followed methodology is, by far, superior to architectural tracing exercises not using the hierarchy approach. Although time-consuming, the authors believe that the BS methodology has greatly improved both the accuracy and objectivity of the observations, and improved current understanding of the rock record in a similar way as it did for understanding the fluvial rock record (e.g. Holbrook, 2001).

CONCLUSIONS

The complex structure of amalgamated supercritical-flow bedforms in the inferred channel–lobe transition-zone (CLTZ) at the base of slope of a deepwater delta of the Sant Llorenç del Munt delta complex were studied by examination of their bounding surface hierarchy.

Chute and pool bedform architecture is interpreted to be formed by mouthbar related hydraulic jumps, which were compared with cyclic step and antidune-bedform characteristics by combining architectural studies with facies analysis, and by comparing these with supercritical-flow bedform experiments and examples from the modern environment.

Diagnostic features of solitary hydraulic jumps include the presence of a deep scour at the downslope end of irregularly undulating fourth-order bounding surfaces (BS) in a morphodynamic setting characterized by antidunes.

Important characteristics for recognizing antidunes are upslope thinning beds, wavy truncation surfaces and upslope directed palaeoflow in the backset beds. Characteristics for chute and pool and/or cyclic step bedforms are long traceable fourth-order BS associated with downslope-thinning backset-beds with local

slumped strata and downslope-directed flow indicators.

The usefulness of the bounding surface hierarchy approach (cf. Miall, 1985) for turbidite deposits lies in the careful evaluation of the spatial extent of bounding surfaces, where these are easily overlooked in complex architectures in the CLTZ of deep-water deltas as described here.

ACKNOWLEDGEMENTS

M. Lopez-Blanco and P. Arbues are thanked for introducing us to the field sites and discussion. Parts of this study (contribution JL) were funded by the German Research Foundation (DFG, Grant LA4422/1-1). Kick Kleverlaan, Hannah Brooks and Arnoud Slootman are thanked for their critical reading, which improved the final text. The senior author acknowledges generous research funding by Exxon Mobile Upstream Research Company.

REFERENCES

Alexander, J., **Bridge, J.S.**, **Cheel, R.J.** and **Leclair, S.F.** (2001) Bedforms and associated sedimentary structures formed under water flows over aggrading sand beds. *Sedimentology*, **48**, 133–152.

Allen, J.R.L. (1968) Flute marks and flow separation. *Nature*, **219**, 602–604.

Allen, J.R.L. (1971) Transverse erosional marks of mud and rock: their physical basis and geological significance. *Sed. Geol.*, **5**, 167–385.

Baas, J.H., **Van Kesteren, W.** and **Postma, G.** (2004) Deposits of depletive, quasi-steady high-density turbidity currents: a flume analogue of bed geometry, structure and texture. *Sedimentology*, **51**, 1053–1089.

Bain, H.A. and **Hubbard, S.M.** (2016) Stratigraphic evolution of a long-lived submarine channel system in the Late Cretaceous Nanaimo Group, British Columbia, Canada. *Sed. Geol.*, **337**, 113–132.

Bhattacharya, J.P. and **Maceachern, J.A.** (2009) Hyperpycnal rivers and prodeltaïc shelves in the cretaceous seaway of North America. *J. Sed. Res.*, **79**, 184–209.

Bouma, A.H. (1962) *Sedimentology of Some Flysch Deposits: A Graphic Approach to Facies Interpretation*. Elsevier, Amsterdam, 168 pp.

Cabello, P., **Falivene, O.**, **López-Blanco, M.**, **Howell, J.**, **Arbués, P.** and **Ramos, E.** (2010) Modelling facies belt distribution in fan deltas coupling sequence stratigraphy and geostatistics: the Eocene Sant Llorenç del Munt example (Ebro foreland basin, NE Spain). *Mar. Petrol. Geol.*, **27**, 254–272.

Cartigny, M.J.B. and **Postma, G.** (2016) Turbidity current bedforms. In: *Atlas of Bedforms in the Western Mediterranean* (Eds Guillén, J., Acosta-Yepes, J., Chiocci, F.L. and Palanques, A.), pp. 29–33. Springer, Cham.

Cartigny, M.J.B., **Eggenhuisen, J.T.**, **Hansen, E.W.M.** and **Postma, G.** (2013) Concentration-dependent flow stratification in experimental high-density turbidity currents and their relevance to turbidite facies models. *J. Sed. Res.*, **83**, 1046–1064.

Cartigny, M.J., **Ventra, D.**, **Postma, G.** and **van den Berg, J.H.** (2014) Morphodynamics and sedimentary structures of bedforms under supercritical-flow conditions: new insight from flume experiments. *Sedimentology*, **61**, 712–748.

Clare, M.A., **Clarke, J.H.**, **Talling, P.J.**, **Cartigny, M.J.B.** and **Pratomo, D.G.** (2016) Preconditioning and triggering of offshore slope failures and turbidity currents revealed by most detailed monitoring yet at a fjord-head delta. *Earth Planet. Sci. Lett.*, **450**, 208–220.

Cornard, P.H. and **Pickering, K.T.** (2019) Supercritical-flow deposits and their distribution in a submarine channel system, Middle Eocene, Ainsa basin, Spanish Pyrenees. *J. Sed. Res.*, **89**, 576–597.

Covault, J.A., **Kostic, S.**, **Paull, C.K.**, **Ryan, H.F.** and **Fildani, A.** (2014) Submarine channel initiation, filling and maintenance from sea-floor geomorphology and morphodynamic modelling of cyclic steps. *Sedimentology*, **61**, 1031–1054.

Cullis, S., **Colombera, L.**, **Patacci, M.** and **McCaffrey, W.D.** (2018) Hierarchical classifications of the sedimentary architecture of deep-marine depositional systems. *Earth-Sci. Rev.*, **179**, 38–71.

Deptuck, M.E., **Piper, D.J.W.**, **Savoye, B.** and **Gervais, A.** (2008) Dimensions and architecture of late Pleistocene submarine lobes off the northern margin of East Corsica. *Sedimentology*, **55**, 869–898.

Dietrich, P., **Ghienne, J.-F.**, **Normandeau, A.** and **Lajeunesse, P.** (2016) Upslope-migrating bedforms in a proglacial sandur delta: cyclic steps from river-derived underflows? *J. Sed. Res.*, **86**, 113–123.

Dżułyński, S. and **Sanders, J.E.** (1962) Current marks on firm mud bottoms. *Trans. Connecticut Acad. Arts Sci.*, **42**, 57–96.

Eagar, R.M.C., **Baines, J.G.**, **Collinson, J.D.**, **Hardy, P.G.**, **Ololo, S.A.** and **Pollard, J.E.** (1985) Trace fossil assemblages and their occurrence in Silecia (mid Carboniferous) deltaic sediments of the central Pennine Basin. In: *Biogenic Structures: Their Use in Interpreting Depositional Environments* (Ed. Curran, L.A.). *SEPM Spec. Publ.*, **35**, 99–150.

Fedele, J. (2002) Bedforms and gravity underflows in marine environments. PhD Thesis, University of Illinois, Urbana-Champaign, IL, 402 pp.

Fedele, J., **Hoyal, D.**, **Barnaal, Z.**, **Tulenko, J.** and **Awalt, S.** (2016) Bedforms created by gravity flows. In: *Autogenic Dynamics and Self-Organization in Sedimentary Systems* (Eds Budd, D., Hajek, E. and Purkis, S), *SEPM, Spec. Publ.*, **106**, pp. 95–121. https://doi.org/10.2110/sepmsp.106.12

Gervais, A., **Savoye, B.**, **Piper, D.J.W.**, **Mulder, T.**, **Cremer, M.** and **Pichevin, L.** (2004) Present morphology and depositional architecture of a sandy confined submarine system: the Golo turbidite system (eastern margin of Corsica). In: *Confined Turbidite Systems* (Eds Lomas, S.A. and Joseph, P.), *Geol. Soc. Spec. Publ.*, **222**, pp. 59–89.

Hage, S., **Cartigny, M.J.B.**, **Sophie, H.**, **Matthieu, J.B.C.**, **Michael, A.C.**, **Esther, J.S.**, **Daniela, V.**, **John, E.H.C.**, **Stephen, M.H.**, **Peter, J.T.**, **Gwyn Lintern, D.**, **Cooper, D.S.**, **Rebecca, G.E.**, **Mark, E.V.**, **James, E.H.**, **Miwa, Y.**, **Daniel, R.P.**, **Jamie, L.H.**, **Maria, A-Z.**, **Age, J.V.**, *et al.* (2018) How to recognize crescentic bedforms formed by supercritical turbidity currents in the geologic record: insights from active submarine channels. *Geology*, **46**, 563–566. https://doi.org/10.1130/G40095.1.

Hamilton, P.B., **Strom, K.B.** and **Hoyal, D.C.J.D.** (2015) Hydraulic and sediment transport properties of autogenic avulsion cycles on submarine fans with supercritical distributaries. *J. Geophys. Res. Earth Surf.*, **120**, 1369–1389.

Hamilton, P.B., **Gaillot, G.**, **Strom, K.B.**, **Fedele, J.** and **Hoyal, D.C.J.D.** (2017) Linking hydraulic properties in supercritical submarine distributary channels to depositional lobe geometry. *J. Sed. Res.*, **87**, 935–950.

Hand, B.M. (1974) Supercritical flow in density currents. *J. Sed. Res.*, **44**, 637–648.

Holbrook, J. (2001) Origin, genetic relationships, and stratigraphy over the continuum of fluvial channel form bounding surfaces: an illustration from middle Cretaceous strata, southeastern Colorado. *Sed. Geol.*, **2001**, 179–222.

Hoyal, D.C.J.D. and **Sheets, B.A.** (2009) Hydraulic jumps as controls on the evolution of distributary channel networks on experimental submarine fans. In: 33rd International Association of Hydraulic Research Congress, Vancouver BC. Canada, pp. 5474–5481.

Hughes Clarke, J.E. (2016) First wide-angle view of channelized turbidity currents links migrating cyclic steps to flow characteristics. *Nat. Commun.*, **7**, 11896. https://doi.org/10.1038/ncomms11896.

Hughes Clarke, J.E., **Brucker, S.**, **Muggah, J.**, **Hamilton, T.**, **Cartwright, D.**, **Church, I.** and **Kuus, P.** (2012) Temporal progression and spatial extent of mass wasting events on the Squamish prodelta slope. In: *Landslides and Engineered Slopes: Protecting Society through Improved Understanding* (Eds Eberhardr, E., Froese, C., Turner, K. and Leroueil, S.), pp. 1091–1096. Taylor & Francis Group, London, ISBN 978-0-415-62123-6.

Lang, J. and **Winsemann, J.** (2013) Lateral and vertical facies relationships of bedforms deposited by aggrading supercritical flows: from cyclic steps to humpback dunes. *Sed. Geol.*, **296**, 36–54.

Lang, J., **Brandes, C.** and **Winsemann, J.** (2017) Erosion and deposition by supercritical density flows during channel avulsion and backfilling: field examples from coarse-grained deepwater channel-levee complexes (Sandino Fore-arc Basin, southern Central America). *Sed. Geol.*, **349**, 79–102.

Leclair, S.F. and **Arnott, R.W.C.** (2005) Parallel lamination formed by high-density turbidity currents. *J. Sed. Res.*, **75**, 1–5. https://doi.org/10.2110/jsr.2005.001.

López-Blanco, M., **Marzo, M.**, **Burbank, D.W.**, **Vergés, J.**, **Roca, E.**, **Anadón, P.** and **Piña, J.** (2000a) Tectonic and climatic controls on the development of foreland fan deltas: Montserrat and Sant Llorenç del Munt systems (Middle Eocene, Ebro Basin, NE Spain). *Sed. Geol.*, **138**, 17–39.

López-Blanco, M., **Marzo, M.** and **Piña, J.** (2000b) Transgressive-regressive sequence hierarchy of foreland, fan-delta clastic wedges (Montserrat and Sant Llorenç del Munt, Middle Eocene, Ebro Basin, NE Spain). *Sed. Geol.*, **138**, 41–69.

López-Blanco, M., **Piña, J.** and **Marzo, M.** (2000c) Anatomy of regressive tracts in a regressive sequence set: Vilomara unit, Sant Llorenç del Munt, Ebro Basin, NE Spain. *Sed. Geol.*, **138**, 143–159.

Lowe, D.R. (1982) Sedimentary gravity flows: II. Depositional models with special reference to the deposits of high density turbidity currents. *J. Sed. Petrol.*, **52**, 279–297.

MacDonald, R.G., **Alexander, J.**, **Bacon, J.C.** and **Cooker, M.J.** (2009) Flow patterns, sedimentation and deposit architecture under a hydraulic jump on a non-eroding bed: defining hydraulic-jump unit bars. *Sedimentology*, **56**, 1346–1367.

Marzo, M. and **Anadón, P.** (1988) Anatomy of a conglomeratic fan-delta complex: the Eocene Montserrat Conglomerate, Ebro basin, north-eastern Spain. In: *Fan Deltas and Related Systems* (Eds Nemec, W. and Steel, R.J.), *Sedimentology and Tectonic Settings*, Blackie Publishing Group, London, pp. 318–340.

Massari, F. (2017) Supercritical-flow structures (backset-bedded sets and sediment waves) on high-gradient clinoform systems influenced by shallow-marine hydrodynamics. *Sed. Geol.*, **360**, 73–95.

Miall, A.D. (1985) Architectural-element analysis: a new method of facies analysis applied to fluvial deposits. *Earth-Sci. Rev.*, **22**, 261–308.

Mutti, E., **Davoli, G.**, **Tinterri, R.** and **Zavala, C.** (1996) The importance of ancient fluvio-deltaic systems dominated by catastrophic flooding in tectonically active basins. *Sci. Geol. Mem.*, **48**, 233–291.

Mutti, E., **Tinterri, R.**, **Benevelli, G.**, **Di Biase, D.** and **Cavanna, G.** (2003) Deltaic, mixed and turbidite sedimentation of ancient foreland basins. *Mar. Petrol. Geol.*, **20**, 733–755.

Ono, K. and **Plink-Björklund, P.** (2018) Froude supercritical flow bedforms in deep-water slope channels? Field examples in conglomerates, sandstones and fine-grained deposits. *Sedimentology*, **65**, 639–669.

Paull, C.K., **Caress, D.W.**, **Ussler, W.**, **Lundsten, E.** and **Meiner-Johnson, M.** (2011) High-resolution bathymetry of the axial channels within Monterey and Soquel submarine canyons, offshore central California. *Geosphere*, **7**, 1077–1101.

Paull, C.K. and **Talling, P.J.** *et al.* (2018) Powerful turbidity currents driven by dense basal layers. *Nat. Commun.*, **9**, 1–9. https://doi.org/10.1038/s41467-018-06254-6.

Peakall, J. *et al.* (2020) An integrated process-based model of flutes and tool marks in deep-water environments: implications for palaeo-hydraulics, the Bouma sequence, and hybrid event beds. *Sedimentology*, accepted.

Petter, A.L. and **Steel, R.J.** (2006) Hyperpycnal flow variability and slope organization on an Eocene shelf margin, Central Basin, Spitsbergen. *Am. Asso. Petrol. Geol. Bull.*, **90**, 1451–1472.

Pickering, K.T. and **Cantalejo, B.** (2015) Deep-marine environments of the Middle EoceneUpper Hecho Group, Spanish Pyrenees: introduction. *Earth-Sci. Rev.*, **144**, 1–9.

Plink-Björklund, P. and **Steel, R.J.** (2004) Initiation of turbidity currents: outcrop evidence for Eocene hyperpycnal flow turbidites. *Sed. Geol.*, **165**, 29–52.

Pohl, F. (2019) Turbidity currents and their deposits in abrupt morphological transition zones. PhD Thesis, Utrecht Studies in Earth Sciences, 181, 210 pp. Utrecht University, Utrecht.

Ponce, J.J. and **Carmona, N.** (2011) Coarse-grained sediment waves in hyperpycnal clinoform systems, Miocene of the Austral foreland basin, Argentina. *Geology*, **39**, 763–766.

Postma, G. (1990) Depositional architecture and facies of river and fan deltas: a synthesis. In: *Coarse Grained Deltas* (Eds A. Colella and D.B. Prior). *I.A.S. Spec. Publ.*, **10**, pp. 13–27, Blackwell, Oxford.

Postma, G. and **Cartigny, M.J.B.** (2014) Supercritical and subcritical turbidity currents and their deposits- A synthesis. *Geology*, **42**, 987–990.

Postma, G. and **Kleverlaan, K.** (2018) Supercritical flows and their control on the architecture and facies of small-radius sand-rich fan lobes. *Sed. Geol.*, **364**, 53–70.

Postma, G., **Nemec, W.** and **Kleinspehn, K.L.** (1988) Large floating clasts in turbidites: a mechanism for their emplacement. *Sed. Geol.*, **58**, 47–61.

Postma, G., **Cartigny, M.** and **Kleverlaan, K.** (2009) Structureless, coarse-tail graded Bouma Ta formed by internal hydraulic jump of the turbidity current? *Sed. Geol.*, **219**, 1–6.

Postma, G., **Kleverlaan, K.** and **Cartigny, M.J.B.** (2014) Recognition of cyclic steps in sandy and gravelly turbidite sequences and consequences for the Bouma facies model. *Sedimentology*, **61**, 2268–2290.

Postma, G., **Hoyal, D.C.J.D.**, **Abreu, V.**, **Cartigny, M.**, **Demko, T.**, **Fedele, J.**, **Kleverlaan, K.** and **Pederson, K.H.** (2016) Morphodynamics of supercritical turbidity currents in the channel-lobe transition zone. In: *Submarine Mass Movements and Their Consequences* (Eds Lamarche, G. and Mountjoy, J.), pp. 469–478. Springer, Dordrecht.

Sequeiros, O.E., **Spinewine, B.**, **Beaubouef, R.T.**, **Sun, T.**, **Garcia, M.H.** and **Parker, G.** (2010) Bedload transport and bed resistance associated with density and turbidity currents. *Sedimentology*, **57**, 1463–1490.

Slootman, A. and **Cartigny, M.J.B.** (2020). Cyclic steps: Review and aggradation-based classification. *Earth-Science Reviews*, **201**, 102949.

Slootman, A., **Cartigny, M.J.B.** and **Vellinga, A.** (2019a) Build-up and fill structure: The depositional signature of strongly aggradational chute-and pool bedforms. In: *Marine and River Dune Dynamics*, Symposium extended Abstracts MARID VI, 1-3 April 2019, pp. 1–6, Bremen, Germany.

Slootman, A., **De Boer, P.L.**, **Cartigny, M.J.**, **Samankassou, E.** and **Moscariello, A.** (2019b) Evolution of a carbonate delta generated by gateway-funnelling of episodic currents. *Sedimentology*, **66**, 1302–1340.

Sohn, Y.K. (1997) On traction-carpet sedimentation. *J. Sed. Res.*, **67**3, 502–509.

Spinewine, B., **Sequeiros, O.E.**, **Garcia, M.H.**, **Beaubouef, R.T.**, **Sun, T.** and **Savoye, B.** (2009) Experiments on wedge-shaped deep sea sedimentary deposits in minibasins and/or on channel levees emplaced by turbidity currents. Part II. Morphodynamic evolution of the wedge and of the associated bedforms. *J. Sed. Res.*, **79**, 608.

Sprague, A.R.G., **Garfield, T.R.**, **Goulding, F.J.**, **Beaubouef, R.T.**, **Sullivan, M.D.**, **Rossen, C.**, **Cmapion, K.M.**, **Sickafoose, D.K.**, **Abreu, V.**, **Schellpeper, M.E.**, **Jensen, G.N.**, **Jennette, D.C.**, **Pirmez, C.**, **Dixon, B.T.**, **Ying, D.**, **Ardill, J.**, **Mohrig, D.C.**, **Porter, M.L.**, **Farrell, M.E.** and **Mellere, D.** (2005). Integrated slope channel depositional models: The key to successful prediction of reservoir presence and quality in offshore West Africa. In: CIPM, Cuarto E-Exitep 2005, February 20–23, 2005, Veracruz, Mexicopp. 1–13.

Steel, R., **Rasmussen, H.**, **Eide, S.**, **Neuman, B.** and **Siggerud, E.** (2000) Anatomy of high sediment supply, transgressive tracts in the Vilomara composite sequence, Sant Llorenç del Munt, Ebro Basin, NE Spain. *Sed. Geol.*, **138**, 161–177.

Talling, P.J., **Masson, D.G.**, **Sumner, E.J.** and **Malgesini, G.** (2012) Subaqueous sediment density flows: depositional processes and deposit types. *Sedimentology*, **59**, 1937–2003.

Vendettuoli, D., **Clare, M.A.**, **Hughes Clarke, J.E.**, **Vellinga, A.**, **Hizzeta, J.**, **Hage, S.**, **Cartigny, M.J.B.**, **Talling, P.J.**, **Waltham, D.**, **Hubbard, S.M.**, **Stacey, C.** and **Lintern, D.G.** (2019) Daily bathymetric surveys document how stratigraphy is built and its extreme incompleteness in submarine channels. *Earth Planet. Sci. Lett.*, **515**, 231–247.

Ventra, D., **Cartigny, M.J.B.**, **Bijkerk, J.F.** and **Acikalin, S.** (2015) Supercritical-flow structures on a Late Carboniferous delta front: sedimentologic and paleoclimatic significance. *Geology*, **43**, 731–734.

Zavala, C. and **Arcuri, M.** (2006) Intrabasinal and extrabasinal turbidites: origin and distinctive characteristics. *Sed. Geol.*, **337**, 36–54.

Manuscript received 25 February 2020; revision accepted 16 March 2020